

## Diatom transcriptional and physiological responses to changes in iron bioavailability across ocean provinces

Natalie R. Cohen<sup>1</sup>, Kelsey Ellis<sup>1</sup>, Robert H. Lampe<sup>1</sup>, Heather McNair<sup>2</sup>, Benjamin Twining<sup>3</sup>, Maria T. Maldonado<sup>4</sup>, Mark A. Brzezinski<sup>2</sup>, Fedor I. Kuzminov<sup>5</sup>, Kimberlee Thamatrakoln<sup>5</sup>, Claire P. Till<sup>6, 7</sup>, Kenneth Bruland<sup>6</sup>, William Sunda<sup>1</sup>, Sibel Bargu<sup>8</sup>, Adrian Marchetti<sup>1\*</sup>

<sup>1</sup>Marine Sciences, University of North Carolina at Chapel Hill, United States, <sup>2</sup>The Marine Science Institute and the Department of Ecology Evolution and Marine Biology, University of California, Santa Barbara, United States, <sup>3</sup>Bigelow Laboratory For Ocean Sciences, United States, <sup>4</sup>Department of Earth, Ocean, and Atmospheric Sciences, University of British Columbia, Canada, <sup>5</sup>Department of Marine and Coastal Sciences, Rutgers University, The State University of New Jersey, United States, <sup>6</sup>Department of Ocean Sciences, University of California, Santa Cruz, United States, <sup>7</sup>Chemistry Department, Humboldt State University, United States, <sup>8</sup>Department of Oceanography and Coastal Sciences, Louisiana State University, United States

*Submitted to Journal:*  
Frontiers in Marine Science

*Specialty Section:*  
Marine Ecosystem Ecology

*ISSN:*  
2296-7745

*Article type:*  
Original Research Article

*Received on:*  
13 Aug 2017

*Accepted on:*  
26 Oct 2017

*Provisional PDF published on:*  
26 Oct 2017

*Frontiers website link:*  
[www.frontiersin.org](http://www.frontiersin.org)

*Citation:*  
Cohen NR, Ellis K, Lampe RH, McNair H, Twining B, Maldonado MT, Brzezinski MA, Kuzminov FI, Thamatrakoln K, Till CP, Bruland K, Sunda W, Bargu S and Marchetti A(2017) Diatom transcriptional and physiological responses to changes in iron bioavailability across ocean provinces. *Front. Mar. Sci.* 4:360. doi:10.3389/fmars.2017.00360

*Copyright statement:*  
© 2017 Cohen, Ellis, Lampe, McNair, Twining, Maldonado, Brzezinski, Kuzminov, Thamatrakoln, Till, Bruland, Sunda, Bargu and Marchetti. This is an open-access article distributed under the terms of the [Creative Commons Attribution License \(CC BY\)](https://creativecommons.org/licenses/by/4.0/). The use, distribution and reproduction in other forums is permitted, provided the original author(s) or licensor are credited and that the original publication in this journal is cited, in accordance with accepted academic practice. No use, distribution or reproduction is permitted which does not comply with these terms.

This Provisional PDF corresponds to the article as it appeared upon acceptance, after peer-review. Fully formatted PDF and full text (HTML) versions will be made available soon.

Provisional

1 **Diatom transcriptional and physiological responses to changes**  
2 **in iron bioavailability across ocean provinces**

3  
4 Natalie R. Cohen<sup>1</sup>, Kelsey A. Ellis<sup>1</sup>, Robert H. Lampe<sup>1</sup>, Heather McNair<sup>2</sup>, Benjamin S.  
5 Twining<sup>3</sup>, Maria T. Maldonado<sup>4</sup>, Mark A. Brzezinski<sup>2</sup>, Fedor I. Kuzminov<sup>5</sup>, Kimberlee  
6 Thamatrakoln<sup>5</sup>, Claire P. Till<sup>6,7</sup>, Kenneth W. Bruland<sup>6</sup>, William G. Sunda<sup>1</sup>, Sibel Bargu<sup>8</sup>,  
7 Adrian Marchetti<sup>1\*</sup>

8  
9 <sup>1</sup> Department of Marine Sciences, University of North Carolina at Chapel Hill, Chapel  
10 Hill, NC, USA

11 <sup>2</sup>The Marine Science Institute and the Department of Ecology Evolution and Marine  
12 Biology, University of California, Santa Barbara, CA, USA

13 <sup>3</sup>Bigelow Laboratory for Ocean Sciences, East Boothbay, ME, USA

14 <sup>4</sup>Department of Earth, Ocean, and Atmospheric Sciences, University of British Columbia,  
15 Vancouver, BC, Canada

16 <sup>5</sup>Department of Marine and Coastal Sciences, Rutgers, the State University of New  
17 Jersey, New Brunswick, NJ, USA

18 <sup>6</sup>Department of Ocean Sciences, University of California Santa Cruz, CA, USA

19 <sup>7</sup>Chemistry Department, Humboldt State University, Arcata, CA, USA

20 <sup>8</sup>Department of Oceanography and Coastal Sciences, College of the Coast and  
21 Environment, Louisiana State University, Baton Rouge, LA, USA

22  
23 \*Correspondence:

24 Adrian Marchetti

25 amarchetti@unc.edu

26  
27 **Running title:** Diatom responses to changes in iron bioavailability

28  
29 **Keywords:** diatoms, Thalassiosira, Pseudo-nitzschia, iron, metatranscriptomics,  
30 California Upwelling Zone, Northeast Pacific Ocean

31  
32

33 **Abstract**

34 Changes in iron (Fe) bioavailability influence diatom physiology and community  
35 composition, and thus have a profound impact on primary productivity and ecosystem  
36 dynamics. Iron limitation of diatom growth rates has been demonstrated in both oceanic  
37 and coastal waters of the Northeast Pacific Ocean and is predicted to become more  
38 pervasive in future oceans. However, it is unclear how the strategies utilized by  
39 phytoplankton to cope with low Fe bioavailability and resupply differ across these ocean  
40 provinces. We investigated the response of diatom communities to variable Fe conditions  
41 through incubation experiments performed in the Fe mosaic of the California Upwelling  
42 Zone and along a natural Fe gradient in the Northeast Pacific Ocean. Through coupling  
43 gene expression of two dominant diatom taxa (*Pseudo-nitzschia* and *Thalassiosira*) with  
44 biological rate process measurements, we provide an in-depth examination of the  
45 physiological and molecular responses associated with varying Fe status. Following Fe  
46 enrichment, oceanic diatoms showed distinct differential expression of gene products  
47 involved in nitrogen assimilation, photosynthetic carbon fixation and vitamin production  
48 compared to diatoms from low-Fe coastal sites, possibly driven by the chronic nature of  
49 Fe stress at the oceanic site. Genes of interest involved in Fe and N metabolism  
50 additionally exhibited divergent expression patterns between the two diatom taxa  
51 investigated, demonstrating that diverse diatoms may invoke alternative strategies when  
52 dealing with the identical changes in their environment. We report here several  
53 mechanisms used distinctly by coastal or oceanic diatom communities as well as  
54 numerous taxa-specific strategies for coping with Fe stress and rearranging nutrient  
55 metabolism following Fe enrichment.

56

Provisional

## 57 **Introduction**

58 Phytoplankton growth is limited by iron (Fe) availability in approximately 30-  
59 40% of the ocean (Moore et al., 2002, 2004). The subarctic Northeast (NE) Pacific Ocean  
60 is one of the most well-characterized of these high-nutrient, low chlorophyll (HNLC)  
61 regions. Productivity in the NE Pacific Ocean remains low as a result of low Fe  
62 concentrations regardless of sufficient nitrate ( $\text{NO}_3^-$ ) levels and is typically dominated by  
63 small cells such as the cyanobacterium *Synechococcus* and eukaryotic picophytoplankton  
64 (Varela and Harrison, 1999). In this region, Fe is supplied to surface waters mainly  
65 through atmospheric deposition of dust from arid continental regions and volcanic  
66 emissions, with Fe inputs from continental margin sediments fueling winter  
67 phytoplankton blooms when atmospheric deposition is low (Lam et al., 2006; Lam and  
68 Bishop, 2008). A gradient in surface nutrient concentrations is observed from this oceanic  
69 region eastwards towards the continent; bioavailable Fe increases and supports higher  
70 phytoplankton biomass while  $\text{NO}_3^-$  concentrations in the upper mixed layer decrease to  
71 limiting levels on the continental shelf (Harris et al., 2009; Ribalet et al., 2010; Taylor  
72 and Haigh, 1996).

73  
74 Iron-limited growth of phytoplankton may also occur in coastal waters, notably in  
75 regions of the California Upwelling Zone (CUZ; Hutchins *et al.* 1998; Bruland *et al.*  
76 2001). These regions of the CUZ are characterized by high concentrations of upwelled  
77 macronutrients, but relatively low dissolved Fe (dFe) such that phytoplankton blooms  
78 ultimately become Fe-stressed. Low Fe levels result from the lack of Fe inputs from  
79 rivers and narrow continental shelves that prevent mixing of upwelled water with Fe  
80 derived from Fe-rich shelf sediments (Bruland et al., 2001; Johnson et al., 1999) and  
81 consequently, the primary Fe source in the CUZ is winter river sediment deposition  
82 (Chase et al., 2005; Hutchins et al., 2002).

83  
84 Phytoplankton that subsist in Fe-limited environments are equipped with  
85 strategies to sustain growth during periods of physiological Fe stress and to rapidly  
86 respond to sudden increases in bioavailable Fe. Strategies employed by phytoplankton  
87 include replacement of Fe-containing proteins with Fe-independent ones to decrease  
88 cellular Fe requirements (Allen et al., 2008; La Roche et al., 1996; Lommer et al., 2012;  
89 Peers and Price, 2006), increasing Fe uptake rates through induction of high affinity Fe  
90 uptake systems (Maldonado and Price, 2001; Morrissey et al., 2015) and using Fe storage  
91 through specialized proteins or vacuoles (Marchetti et al., 2009; Nuester et al., 2012). In  
92 some diatom laboratory isolates and natural communities, these low-Fe strategies are  
93 rapidly reversed when Fe concentrations increase (Kustka et al., 2007; Lommer et al.,  
94 2012), whereas in others these strategies are permanent adaptations (Lommer et al., 2010;  
95 Marchetti et al., 2012). Phytoplankton species from low-Fe oceanic environments  
96 generally have lower growth requirements for cellular Fe than species from higher Fe  
97 coastal waters, largely linked to differences in Fe-containing photosynthetic proteins and  
98 complexes (Behrenfeld and Milligan, 2013; Peers and Price, 2006; Strzepek and  
99 Harrison, 2004; Sunda and Huntsman, 1995). While we have an understanding of how a  
100 few phytoplankton species alter their nutrient metabolism in response to chronic Fe  
101 limitation from laboratory experiments, how the nutrient strategies invoked by

102 intermittently Fe-limited coastal taxa might differ from those used by species residing in  
103 chronically Fe-limited regions of the open ocean has not been directly compared.

104

105 A large amount of genetic diversity exists among diatom taxa, possibly due to  
106 differences in environmental pressures at the time of evolutionary emergence (Armbrust,  
107 2009; Rabosky and Sorhannus, 2009; Sims et al., 2006). A genomic comparison between  
108 the evolutionarily older centric *Thalassiosira pseudonana* and the more recently evolved  
109 pennate *Phaeodactylum tricornutum* demonstrates the two diatoms share only 57% of  
110 their genes with each other, suggesting a tremendous amount of genomic diversity exists  
111 between members of these two diatom lineages (Bowler et al., 2008). Furthermore it is  
112 often observed that pennate diatoms, especially those belonging to the genus *Pseudo-*  
113 *nitzschia*, tend to dominate large Fe-induced blooms in HNLC waters (de Baar et al.,  
114 2005; Marchetti et al., 2012). These observations may suggest that the pennate diatoms  
115 have evolved distinct strategies for optimizing their potential for rapid growth when  
116 transitioning from low to relatively high Fe conditions, resulting in a competitive  
117 advantage over older lineages of diatoms as well as other types of phytoplankton.

118

119 To better understand whether major diatom genera from coastal and oceanic  
120 regions differ in their gene expression responses to changes in Fe availability, a  
121 comparative analysis across distinct nutrient regimes was performed through a  
122 combination of metatranscriptomic and physiological approaches. Microcosm incubation  
123 experiments were conducted at geographically diverse sites with different Fe regimes,  
124 macronutrient concentrations, and phytoplankton community compositions – at an Fe-  
125 limited oceanic site and a coastal site in the subarctic NE Pacific Ocean, and at three  
126 biogeochemically distinct sites within the Fe mosaic of the coastal California Upwelling  
127 Zone (CUZ). For our study, we focused on the changes in gene expression patterns  
128 between two dominant taxa across all sites – the pennate diatom *Pseudo-nitzschia* and the  
129 centric diatom *Thalassiosira*. These two taxa were classified by the *Tara Oceans*  
130 circumnavigation expedition to be two of the eight most abundant diatom genera in the  
131 global ocean (Malviya et al., 2016). Given the large amount of genetic and physiological  
132 variation observed between major diatom groups (Alexander et al., 2015; Bowler et al.,  
133 2008; Marchetti et al., 2009; Sutak et al., 2012), differences in molecular responses to  
134 changing Fe availabilities across the NE Pacific Ocean and CUZ were anticipated.

135

## 136 **Materials and Methods**

### 137 *Experimental Design*

138 Incubation experiments were conducted on two separate cruises: within regions of  
139 the CUZ during July 3-26<sup>th</sup> 2014 onboard the *R/V Melville* and along the Line-P transect  
140 of the subarctic NE Pacific Ocean during June 7-23<sup>rd</sup> 2015 onboard the *Canadian Coast*  
141 *Guard Ship (CCGS) John P. Tully* (Fig. 1). The incubated phytoplankton community  
142 response was assessed using a combination of physiological measurements and  
143 metatranscriptomics to examine the effects of Fe status on diatom physiology and gene  
144 expression. Each experiment included three treatments: 1) a 5 nmol L<sup>-1</sup> FeCl<sub>3</sub> addition

145 (Fe), 2) a 200 nmol L<sup>-1</sup> desferroxamine B (DFB) addition, and 3) an unamended control  
146 (Ctl), each sampled at two time points.

147

148 During the CUZ cruise, three incubation experiments were performed at separate  
149 locations corresponding to distinct Fe and macronutrient regimes (Supplemental Table 1),  
150 including sites of high dFe, macronutrients, and phytoplankton biomass (C1: 38°39.30N,  
151 123°39.87W), relatively low dFe, high macronutrients and high phytoplankton biomass  
152 (C2: 38°15.31N, 123°57.98W), and low dFe with high macronutrients and low  
153 phytoplankton biomass (C3: 42°40.00N, 125°0.00W) (Fig. 1). Near-surface seawater was  
154 collected from a depth of approximately 15 m using a trace-metal clean sampling system  
155 consisting of a tow-fish sampler attached to Kevlar<sup>TM</sup> line, PFA Teflon tubing, and a  
156 Teflon dual-diaphragm pump that pumped seawater directly into a positive pressure  
157 trace-metal clean bubble. The seawater was placed in a large 200 L acid-cleaned HDPE  
158 drum for homogenization before being distributed into 10 L flexible acid-cleaned  
159 polyethylene cubitainers (Hedwin Corporation). Cleaning protocols for the cubitainers  
160 included successive soaks in 1.2 mol L<sup>-1</sup> hydrochloric acid (reagent grade) for 3 days, 1.2  
161 mol L<sup>-1</sup> hydrochloric acid (trace metal grade) for 1 week and 0.1 mol L<sup>-1</sup> acetic acid  
162 (trace-metal grade) until use. Prior to filling the cubitainers with seawater, the dilute  
163 acetic acid was removed and the cubitainers were rinsed thoroughly three times with  
164 ambient seawater from the collection site. The primary objective of these experiments  
165 was to elucidate the responses of target diatom genera and the phytoplankton community  
166 to variable Fe conditions. Therefore, sites were targeted that would ensure adequate  
167 macronutrient concentrations to support phytoplankton growth. However at C2, 15 μmol  
168 L<sup>-1</sup> of Si(OH)<sub>4</sub> was added to all cubitainers to support growth of diatoms due to the  
169 initially low Si(OH)<sub>4</sub> concentration (<4.7 μmol L<sup>-1</sup>).

170

171 During the Line-P cruise, incubation experiments were conducted at the low NO<sub>3</sub><sup>-</sup>  
172 coastal station P4 (48°39N, 126°40W; referred to as C4 in this analysis) and at the  
173 chronically Fe-limited, HNLC oceanic station P26, also known as Ocean Station Papa  
174 (OSP, 50°00N, 145°00W; Harrison 2002; referred to as O5). Seawater was collected at  
175 depths corresponding to approximately 30% of incident irradiance (8-12 m) at both  
176 stations using a trace-metal clean sampling system consisting of a Teflon air bellows  
177 pump and PTFE lined Kevlar<sup>TM</sup> tubing attached to a Kevlar<sup>TM</sup> line. The seawater was  
178 pumped directly into 10 L acid-cleaned polyethylene cubitainers placed within an on-  
179 deck trace-metal clean positive pressure flowhood. At site C4, 10 μmol L<sup>-1</sup> of NO<sub>3</sub><sup>-</sup> was  
180 added to all cubitainers to support growth of diatoms due to the initially low NO<sub>3</sub><sup>-</sup>  
181 concentration (<1.5 μmol L<sup>-1</sup>).

182

183 At the start of the experiments, ambient seawater was filtered for all initial  
184 measurements (T<sub>0</sub>). For each incubation experiment, cubitainers were filled to serve as a  
185 control (Ctl) or amended with FeCl<sub>3</sub> or DFB just prior to dawn. All cubitainers were  
186 placed in on-deck Plexiglass incubators with flow-through seawater to maintain near-  
187 ambient surface water temperatures. Incubators were covered with neutral density  
188 screening to achieve approximately 30% of the incident irradiance (Supplemental Fig. 1).  
189 Following 24-96 hours of incubation (Supplemental Table 1; depending on the measured  
190 macronutrient drawdown) the cubitainers for a specific time point were removed from the

191 incubators and filtered immediately. The goal for each time point was to achieve  
192 measureable drawdowns in macronutrients that would infer stimulation of phytoplankton  
193 growth without complete macronutrient depletion. However for some experiments and  
194 time points, depletion of  $\text{NO}_3^-$  or other macronutrients occurred (Supplemental Table 1).  
195 All filtrations were conducted at dawn. Subsamples for dissolved and particulate  
196 nutrients, size-fractionated uptake rates of dissolved inorganic carbon (DIC) and  $\text{NO}_3^-$ ,  
197 size-fractionated chlorophyll *a*,  $F_v/F_m$  and RNA were collected at  $T_0$  and from each  
198 cubitainer according to the protocols described below.  
199

#### 200 *Nutrient concentrations, uptake rates and biogenic silica concentrations*

201 For CUZ experiments, dissolved nitrate and nitrite ( $\text{NO}_3^- + \text{NO}_2^-$ ), phosphate  
202 ( $\text{PO}_4^{3-}$ ), and silicic acid ( $\text{H}_4\text{SiO}_4$ ) concentrations were measured onboard using a Lachat  
203 Quick Chem 8000 Flow Injection Analysis system (Parsons et al., 1984) with detection  
204 limits of  $0.05 \mu\text{M}$  for  $\text{NO}_3^- + \text{NO}_2^-$ ,  $0.03 \mu\text{M}$  for  $\text{PO}_4^{3-}$ , and  $0.2 \mu\text{M}$  for  $\text{H}_4\text{SiO}_4$  (Bruland  
205 et al., 2008). Particles were removed by filtration through a Whatman GF/F filter (25  
206 mm). Reference standards for nutrients in seawater were run for quality control. During  
207 Line-P sampling, approximately 15 mL of seawater was filtered through a Whatman  
208 GF/F filter into acid-rinsed polypropylene tubes and frozen at  $-20^\circ\text{C}$  in aluminum blocks  
209 until onshore analysis. Shortly following the cruise, the dissolved  $\text{NO}_3^- + \text{NO}_2^-$ ,  $\text{PO}_4^{3-}$ ,  
210 and  $\text{H}_4\text{SiO}_4$  concentrations were determined using an Astoria nutrient analyzer (Barwell-  
211 Clarke and Whitney, 1996). Nutrient detection limits were  $0.2 \mu\text{M}$  for  $\text{NO}_3^- + \text{NO}_2^-$ ,  $0.02$   
212  $\mu\text{M}$  for  $\text{PO}_4^{3-}$ , and  $0.5 \mu\text{M}$  for  $\text{H}_4\text{SiO}_4$  (Frank Whitney and Mark Belton [IOS], pers.  
213 comm.).  
214

215 For biogenic silica (bSi) measurements, 335 mL (CUZ) or 250 mL (Line P) of  
216 seawater was filtered onto polycarbonate filters ( $1.2 \mu\text{m}$  pore size for CUZ and  $0.6 \mu\text{m}$   
217 pore size for Line-P, 25 mm), digested with NaOH in Teflon tubes, and measured with  
218 the colorimetric ammonium molybdate method (Krause et al., 2013).  
219

220 Size-fractionated particulate nitrogen (PN), particulate carbon (PC), and  $\text{NO}_3^-$   
221 uptake rates were obtained by adding  $^{15}\text{N}$ - $\text{NaNO}_3$  to 618 mL subsample of experimental  
222 seawater placed within clear polycarbonate bottles. The concentration of  $\text{NO}_3^-$  added  
223 with the radiotracer was no more than 10% of ambient  $\text{NO}_3^-$  level within CUZ  
224 incubations, and was  $1 \mu\text{mol L}^{-1}$  within Line-P incubations (corresponding to  $\text{NO}_3^-$  levels  
225 of 68% at  $T_0$  and 10% within  $\text{NO}_3^-$ -amended incubations at C4, and approximately 10%  
226 at O5). DIC uptake within Line-P incubations was measured by additionally spiking  
227 subsamples with  $120 \mu\text{mol L}^{-1}$   $\text{NaH}^{13}\text{CO}_3$ . Bottles were incubated in the same flow-  
228 through Plexiglass incubators where cubitainers were kept. Following 8 h of incubation,  
229 seawater samples were filtered in series through a polycarbonate filter ( $5 \mu\text{m}$  pore size,  
230 47 mm) via gravity filtration, and then through a pre-combusted ( $450^\circ\text{C}$  for 5 h) GF/F  
231 filter by gentle vacuum ( $< 100 \text{ mg Hg}$ ). Particulates collected on the  $5 \mu\text{m}$  polycarbonate  
232 filter were then rinsed onto a separate pre-combusted GF/F filter using an artificial saline  
233 solution. Filters were stored at  $-20^\circ\text{C}$  until onshore analysis. In the laboratory, filters were  
234 heated to  $60^\circ\text{C}$  for 24 hours and pelletized in tin capsules (Elemental Microanalysis) in  
235 preparation for analysis of the atom %  $^{15}\text{N}$ , atom %  $^{13}\text{C}$  (for Line-P), particulate nitrogen  
236 (PN) and particulate carbon (PC) using an elemental analyzer paired with an isotope ratio

237 mass spectrometer (EA-IRMS). Biomass-normalized  $\text{NO}_3^-$  uptake rates (PN-V $\text{NO}_3$ ) and  
238 DIC uptake rates (PC-VDIC) for the Line-P experiments were obtained by dividing the  
239 measured  $\text{NO}_3^-$  and DIC biological uptake rates by PN and PC concentrations,  
240 respectively.

241  
242 To quantify VDIC in CUZ incubations, incorporation of  $^{14}\text{C}$  was determined using  
243 a protocol adapted from Taylor *et al.* (2013). Briefly, 60 mL of seawater from each  
244 cubitainer was distributed into acid-cleaned light and dark polycarbonate bottles. In each  
245 bottle, 1.2  $\mu\text{Ci}$  of  $\text{NaH}^{14}\text{CO}_3$  was added. Bottles were incubated in the same flow-through  
246 Plexiglass incubators where cubitainers were kept for 6.5-8 h. Following incubation,  
247 samples were filtered through stacked 47mm polycarbonate filters (5  $\mu\text{m}$  and 1  $\mu\text{m}$ )  
248 separated with a mesh spacer during filtration. Filters were vacuum dried, placed in 7 mL  
249 scintillation vials containing 0.5 mL of 6M HCl and permitted to degas for 24h.  
250 Disintegrations per minute (DPM) retained on the filters were measured using a Beckman  
251 Coulter LS 6500 scintillation counter. Reported values are light bottle DPMs minus dark  
252 bottle DPMs. To obtain VDIC, DIC uptake rates were normalized to PC concentrations  
253 obtained as part of the  $\text{NO}_3^-$  uptake measurements within each incubation and size  
254 fraction.

255

#### 256 *Dissolved iron concentrations*

257 Seawater samples for Fe analysis within the CUZ were acidified at sea with the  
258 equivalent of 4 mL 6 N quartz-distilled HCl per L of seawater (pH ~1.7) and stored in  
259 acid-cleaned LDPE bottles for at least two months prior to analysis. Samples were  
260 analyzed using an adaption of Biller and Bruland (2012) as described in (Parker *et al.*,  
261 2016). Briefly, this method involves preconcentrating the Fe from buffered (pH 6.0)  
262 seawater on Nobias-chelate PA1 resin and eluting with 1 N quartz-distilled  $\text{HNO}_3$ . The  
263 eluent was analyzed with a Thermo-Element high resolution XR ICP-MS in counting  
264 mode. Line-P dissolved Fe samples were stored in acid-cleaned LDPE bottles, acidified  
265 post-cruise with Optima-grade HCl (1 mL 12 N HCl per L of seawater), and allowed to  
266 sit for >3 months. Dissolved Fe was measured via ICP-MS by P. Morton at Florida State  
267 University following resin preconcentration using the protocol of Milne *et al.* (2010).

268

#### 269 *Chlorophyll a*

270 Four hundred mL of seawater was gravity-filtered through a polycarbonate filter  
271 (5  $\mu\text{m}$  pore size, 47 mm diameter) followed by vacuum filtration through a GF/F filter  
272 (0.7  $\mu\text{m}$  nominal pore size, 25 mm diameter) using a series filter cascade for size  
273 fractionation. Filters were frozen at  $-80^\circ\text{C}$  until analysis. Chlorophyll *a* extraction was  
274 performed using 90% acetone at  $-20^\circ\text{C}$  for 24 h and the extracted Chl *a* was quantified by  
275 fluorometry with a Turner Designs 10-AU fluorometer using the acidification method  
276 (Parsons *et al.* 1984).

277

#### 278 *Domoic acid*

279 Approximately 250 mL of seawater from each CUZ site was filtered through  
280 GF/F filters (25 mm) via vacuum pressure (<100 mm Hg) and the filters were frozen at -  
281  $80^\circ\text{C}$ . The filters were extracted with 20% methanol (MeOH) in water. The mixture was  
282 sonicated in an ice bath for 2 min at 30-40 W with a Sonicator 3000, followed by

283 centrifugation (10 min, 1399 x g). The supernatant was collected and passed through a  
284 0.22  $\mu\text{m}$  syringe filter. Samples were stored at  $-20^{\circ}\text{C}$  until analysis. Concentrations with a  
285 detection limit of  $0.01 \mu\text{g L}^{-1}$  were obtained using an enzyme-linked immunosorbent  
286 assay (Abraxis, Warminster, PA, USA) following the manufacturer's protocol, including  
287 running each sample in duplicate at several dilutions. Final concentrations ( $\text{pg DA mL}$   
288  $\text{extract}^{-1}$ ) were calculated using the manufacturer supplied analysis spreadsheet.

289

### 290 *Photophysiology*

291 The maximum photochemical yield of PSII ( $F_v/F_m$ ), was measured by fast  
292 repetition rate fluorometry (FRRF) using a custom-built fluorescence-induction and  
293 relaxation system (Kobler et al. 1998; Gorbunov and Falkowski 2005). Before each  
294 measurement, a 5 mL subsample of seawater from each cubitainer was acclimated to low  
295 light for 20 minutes. A saturating pulse ( $20,000 \mu\text{mol photons m}^{-2} \text{s}^{-1}$ ) of blue light (450  
296 nm) was applied to dark-acclimated cells for a duration of 100-200  $\mu\text{s}$ . Measurements  
297 were obtained using the single-turnover flash (STF) setting with the average of 50  
298 iterations for the CUZ experiments, and a single iteration for the Line-P experiments.  
299 Data were blank corrected using  $0.2 \mu\text{m}$  filtered seawater.

300

301

### 302 *RNA extraction and bioinformatic analysis*

303 Phytoplankton in seawater samples were filtered onto  $0.8 \mu\text{m}$  Pall Supor filters  
304 (142 mm) via peristaltic pumping, immediately flash frozen in liquid nitrogen and stored  
305 at  $-80^{\circ}\text{C}$  until extraction onshore. The filters were briefly thawed on ice before being  
306 extracted individually using the ToTALLY RNA Kit (Ambion). The extraction procedure  
307 followed manufacturer protocols with the modified first step of glass bead addition and  
308 vortexing to facilitate disruption of cells. Removal of DNA was performed with one  
309 round of DNase I (Ambion) incubation. For the Line P experiments, due to low yields in  
310 treatments, RNA from the triplicate cubitainers was pooled prior to sequencing. Within  
311 CUZ experiments all triplicate incubation samples were sequenced separately. At the  
312 oceanic site O5, RNA yields were too low to successfully sequence metatranscriptomes  
313 at the  $T_1$  timepoint, and consequently, all transcriptomic analyses were performed using  
314 the  $T_0$ ,  $T_2 \text{ Fe}$  and  $T_2 \text{ Ctl}$  treatments. Metatranscriptomic library preparation was performed  
315 with the Illumina TruSeq Stranded mRNA Library Preparation Kit and HiSeq v4  
316 reagents. Samples were barcoded and run across three lanes of Illumina HiSeq 2000 (125  
317 bp, paired-end) yielding on average 23 million paired-end reads per sample  
318 (Supplemental Table 2). The RNA-seq data reported here has been deposited in the  
319 National Center for Biotechnology (NCBI) sequence read archive (SRA) under the  
320 BioProject accession no. PRJNA320398 and PRJNA388329.

321

322 Raw reads were trimmed for quality bases and removal of adapters using  
323 Trimmomatic v0.32 (paired-end mode, adaptive quality trim with 40bp target length and  
324 strictness of 0.6, minimum length of 36bp; Bolger et al. 2014). Trimmed paired reads  
325 were merged into single reads with BBMerge v8.0. For each site, the resulting merged  
326 pairs and non-overlapping paired-end reads were assembled using ABySS v1.5.2 with a  
327 multi-kmer approach (Birol et al., 2009). The different k-mer assemblies were merged to  
328 remove redundant contigs using Trans-ABYSS v1.5.3 (Robertson et al., 2010). Read

329 counts were obtained by mapping raw reads to assembled contigs with Bowtie2 v2.2.6  
330 (end-to-end alignment; Langmead and Salzberg 2012). Alignments were filtered by  
331 mapping quality score (MAPQ) of 10 or higher as determined by SAMtools v1.2 (Li et  
332 al., 2009). Taxonomic and functional annotations were assigned based on sequence  
333 homology to reference databases via BLASTx v2.3.0 with an e-value cutoff of  $10^{-3}$   
334 (Altschul et al., 1990). Functional annotations were assigned according to the top hit  
335 using the Kyoto Encyclopedia of Genes and Genomes (KEGG; Release 75), while  
336 taxonomic assignments were obtained according to the top hit using MarineRefII  
337 (Laboratory of Mary Ann Moran, University of Georgia), a custom-made database  
338 comprised of protein sequences of marine prokaryotes and eukaryotes including all  
339 sequenced transcriptomes from Marine Microbial Eukaryote Transcriptome Sequencing  
340 Project (MMETSP) (Keeling et al. 2014). Taxonomic information was obtained from  
341 NCBI's Taxonomy Database (each isolate in MarineRefII is assigned a NCBI taxonomic  
342 ID). The information from NCBI was manually curated to ensure proper assignment and  
343 use of common phytoplankton taxonomic ranks. For our analysis, we have grouped  
344 diatom-associated sequences at the genus level. Therefore, the patterns in gene  
345 expression observed could be driven by one dominant species or many equally distributed  
346 species belonging to a genus within each site.

347  
348 All diatom-assigned counts were summed to both the genus taxonomic rank and  
349 KEGG Orthology (KO) functional annotation level. For genes of interest without a KO  
350 assignments but with an annotated gene definition (i.e., ISIPs and rhodopsin), raw counts  
351 corresponding to KEGG gene definitions were summed. EdgeR v3.12.0 was used to  
352 calculate *Pseudo-nitzschia*- or *Thalassiosira*-specific normalized fold change and counts-  
353 per-million (CPM) from pairwise comparisons using the exactTest (Klingenberg and  
354 Meinicke, 2017; Robinson et al., 2010; Robinson and Oshlack, 2010; Robinson and  
355 Smyth, 2008). Significance ( $p < 0.05$ ) was calculated with edgeR's estimate of tagwise  
356 dispersions across all samples within CUZ sites. Heatmaps were produced with the R  
357 package pheatmap v1.0.8, and dendrograms created using Euclidean distance and  
358 hierarchical clustering. Assembled contigs, read counts, and functional annotations of  
359 contigs are available at [marchetttilab.web.unc.edu/data](http://marchetttilab.web.unc.edu/data).

360  
361 In order to directly compare transcript abundance across locations and data sets  
362 for principal component analyses (PCA), the assemblies for all sites were merged with  
363 Trans-ABYSS. The removal of redundant contigs was verified with GenomeTools  
364 v.1.5.1. Counts were obtained by aligning raw reads against this merged  
365 metatranscriptome using Salmon v.0.7.3-beta. Normalized counts were then obtained  
366 with edgeR v3.12.0. PCA biplots were created using log-transformed normalized counts  
367 for genes of interest with ggbiplot v.0.5.

368  
369 *Phylogenetic analysis of environmental sequences*

370 Environmental *Pseudo-nitzschia* and *Thalassiosira* contigs functionally annotated  
371 as RubisCO (*RBCL*), rhodopsin (*RHO*), or superoxide dismutase (*SOD*) and containing a  
372 large number of mapped reads were compared to diatom reference sequences for  
373 phylogenetic characterization. Diatom sequences used in reference alignments were  
374 obtained through a sequence homology search using BLASTx v2.2.28 with *Pseudo-*

375 *nitzschia RBCL*, *RHO* and *SOD* against the database MMETSP using an E-value cutoff of  
376  $10^{-5}$  (Altschul et al. 1990). Sequences were aligned using MUSCLE within Geneious  
377 v5.6.4 software (Edgar, 2004).  
378

## 379 **Results**

### 380 *Nutrient regimes of experimental sites*

381 California Upwelling Zone (CUZ) site C1 (Fig. 1) was characterized by high  
382 macronutrient and dFe concentrations in the mixed layer supporting a high biomass,  
383 nutrient-replete phytoplankton community. The community was dominated by  
384 phytoplankton cells in the  $>5 \mu\text{m}$  chlorophyll *a* (chl *a*) size fraction, constituting 88% of  
385 the total chl *a* concentration (Fig. 2B; Supplemental Table 1). Macronutrient  
386 concentrations were rapidly consumed during the first 24 hours of incubation ( $T_1$ ), with  
387 near complete depletion of the  $\text{NO}_3^-$  ( $\leq 1 \mu\text{mol L}^{-1}$  remaining by 48 hours [ $T_2$ ]; Fig. 2A).  
388 The initially Fe-replete phytoplankton community (dFe:  $3.57 \text{ nmol L}^{-1}$ ) was mostly  
389 unaffected by the additions of Fe or DFB as demonstrated through relatively constant  
390  $F_v/F_m$ , phytoplankton biomass, particulate nitrogen (PN)-specific nitrate uptake rates  
391 ( $\text{VNO}_3$ , or nitrate assimilation rates), and particulate carbon (PC)-specific dissolved  
392 inorganic carbon assimilation rates ( $\text{VDIC}$ , or carbon assimilation rates) across treatments  
393 at each time point (Fig. 2B-E). Furthermore, the  $\text{NO}_3\text{:Fe}$  ratio of the initial ( $T_0$ ) seawater  
394 ( $3.8 \mu\text{mol:nmol}$ . Supplemental Table 1) was substantially below the predicted threshold  
395 ratio for eventual Fe stress of  $12 \mu\text{mol:nmol}$  for phytoplankton in this region as proposed  
396 by King and Barbeau (2007), albeit this ratio is subject to variation as a function of  
397 phytoplankton iron demands (Bruland et al., 2001), suggesting this phytoplankton  
398 community was not likely to be driven into Fe limitation prior to complete  $\text{NO}_3^-$   
399 utilization. However, indications of molecular-level responses to Fe and DFB additions  
400 were observed; 74 genes were differentially expressed ( $p < 0.05$ ) in *Pseudo-nitzschia*  
401 between the Fe and DFB treatments (Supplemental Fig. 2A). Fe-stress bioindicator genes  
402 (*FLDA*, *PETE* and *ISIP2A* [Whitney et al., 2011; Morrissey et al., 2015; Graff van  
403 Creveld et al., 2016]) increased in expression following the addition of DFB relative to  
404 the added Fe treatment, suggesting the onset of Fe stress following the addition of DFB  
405 by the end of the first time point.  
406

407 CUZ site C2 was located in close geographical proximity to C1 (Fig. 1), yet  
408 exhibited different mixed layer properties in relation to phytoplankton biomass, silicic  
409 acid ( $\text{Si}[\text{OH}]_4$ ) and dFe concentrations ( $0.44 \text{ nmol L}^{-1}$ ). Nitrate and ortho-phosphate  
410 ( $\text{PO}_4^{3-}$ ) concentrations were similarly high ( $10.3$  and  $0.96 \mu\text{mol L}^{-1}$ , respectively) as  
411 found at site C1, although  $\text{Si}(\text{OH})_4$  levels were appreciably lower ( $4.7 \mu\text{mol L}^{-1}$ ) and  
412 possibly growth-limiting to certain diatoms (Nelson et al., 1996). Therefore, incubations  
413 were amended with  $15 \mu\text{mol L}^{-1}$   $\text{Si}(\text{OH})_4$  to support potential diatom growth with added  
414 Fe (Brzezinski, 1985). Although the chl *a* concentration in the  $>5 \mu\text{m}$  size fraction was  
415 initially  $<1 \mu\text{g L}^{-1}$  and biogenic silica (bSi) concentrations were  $<3 \mu\text{mol L}^{-1}$ , by 48 hours  
416 ( $T_1$ ) the  $>5 \mu\text{m}$  chl *a* fraction reached  $5\text{-}8 \mu\text{g L}^{-1}$  and bSi increased to  $10\text{-}15 \mu\text{mol L}^{-1}$  in  
417 all treatments, accompanied by appreciable decreases in  $\text{NO}_3^-$ ,  $\text{PO}_4^{3-}$ , and  $\text{Si}(\text{OH})_4$   
418 concentrations (Fig. 2 A&B). Since this community quickly depleted  $\text{NO}_3^-$  concentrations

419 during the experimental period, this site presented an opportunity to couple the  
420 physiological indicators of  $\text{NO}_3^-$  stress with N-related transport and assimilation genes  
421 observed to be elevated in  $\text{NO}_3^-$ -starved laboratory diatom cultures (Bender et al., 2014;  
422 Hildebrand, 2005; Rogato et al., 2015; Song and Ward, 2007). Apart from  $F_v/F_m$  reaching  
423 relatively low values in the DFB treatments, indications of Fe stress in bulk physiological  
424 measurements across treatments were absent (Fig. 2C). However, the initial seawater  
425  $\text{NO}_3^-$ :Fe ratio of 23.4  $\mu\text{mol}:\text{nmol}$  suggests this community may have been driven into Fe  
426 limitation provided sufficient  $\text{Si}(\text{OH})_4$  was present. Additionally, a total of 414 *Pseudo-*  
427 *nitzschia*-associated genes were differentially expressed ( $p < 0.05$ ) by  $T_1$  between the Fe  
428 and DFB treatments (Supplemental Fig. 2). This greater number of differentially  
429 expressed genes in *Pseudo-nitzschia* when compared to C1 suggests the C2 diatom  
430 community in the DFB treatment experienced a higher degree of Fe stress during the  
431 incubation period. The initially low dissolved  $\text{Si}(\text{OH})_4$ : $\text{NO}_3^-$  ratio at this site furthermore  
432 implies a possible increase in the Si:N ratios of Fe-stressed diatoms (Brzezinski et al.,  
433 2015; Hutchins and Bruland, 1998; Marchetti and Cassar, 2009). Interestingly,  
434 concentrations of domoic acid (DA), a neurotoxin produced by *Pseudo-nitzschia*, was 90  
435  $\text{pg mL}^{-1}$  in initial seawater ( $T_0$ ) and exceeded 3,000  $\text{pg mL}^{-1}$  in the control treatment by  $T_1$   
436 (Supplemental Fig. 3). This increase in DA concentration may be linked to both the  
437 increase in *Pseudo-nitzschia* abundance and depletion of  $\text{Si}(\text{OH})_4$  resulting in Si-limited  
438 cells which has been shown to greatly enhance DA production (Pan et al., 1996).

439

440 Site C3 (Fig. 1) contained the lowest dFe concentrations (0.31  $\text{nmol L}^{-1}$ ) among  
441 the CUZ sites along with high macronutrient concentrations (17  $\mu\text{mol L}^{-1}$   $\text{NO}_3^-$ , 19  $\mu\text{mol}$   
442  $\text{L}^{-1}$   $\text{Si}(\text{OH})_4$ , and 1.5  $\mu\text{mol L}^{-1}$   $\text{PO}_4^{3-}$ ; Fig. 2A). The corresponding  $\text{NO}_3^-$ :Fe ratio of the  
443 initial seawater was approximately 54.9  $\mu\text{mol}:\text{nmol}$  (Supplemental Table 1). Following  
444 incubation, the chl *a*, bSi, PN-specific  $\text{VNO}_3$ , and PC-specific VDIC were all higher in  
445 the Fe-amended treatment relative to the unamended control by  $T_1$  (Fig. 2 B,D-E). By 72  
446 hours,  $\text{NO}_3^-$  was completely drawn down within the Fe treatment ( $T_2$ ). Despite the  
447 pronounced influence of Fe enrichment on bulk parameters,  $F_v/F_m$  values were only  
448 slightly higher in the Fe treatment than the control, but they were substantially higher  
449 than in the DFB treatment (Fig. 2C). This is likely a reflection of the different  
450 phytoplankton composition at this location compared to site C2, which did not show  
451 indications of an Fe-addition response on the measured bulk parameters, but did  
452 demonstrate elevated  $F_v/F_m$  values in the added Fe treatment. Site C3 represented the  
453 only phytoplankton community in the CUZ that displayed a definite physiological  
454 response to Fe addition relative to the control treatment (Supplemental Table 1). The Fe-  
455 induced molecular response in diatoms was demonstrated by the differential expression  
456 of 458 genes in *Pseudo-nitzschia* and 1,223 genes in *Thalassiosira* between the Fe and  
457 DFB treatments (Supplemental Fig. 2C), and 365 genes in *Pseudo-nitzschia* and 837  
458 genes in *Thalassiosira* between the Fe and Ctl treatments ( $p < 0.05$ ).

459

460 Coastal site C4 was located at station P4 of the Line-P transect in the subarctic  
461 NE Pacific Ocean (Fig. 1). Initial mixed-layer seawater properties were characterized by  
462 low concentrations of macronutrients and dFe, which supported a low phytoplankton  
463 biomass. Nitrate concentrations were initially 1.5  $\mu\text{mol L}^{-1}$  (Fig. 2A). To facilitate a  
464 potential phytoplankton growth response to added Fe, 10  $\mu\text{mol L}^{-1}$  of  $\text{NO}_3^-$  was added to

465 each treatment.  $\text{Si(OH)}_4$  concentrations were also initially low ( $2.2 \mu\text{mol L}^{-1}$ ) and  
466 incubation concentrations dropped to  $<2 \mu\text{mol L}^{-1}$  in most treatments by the second time  
467 point ( $T_2$ ; Fig. 2A). These low concentrations restricted biomass accumulation as bSi  
468 (Fig. 2B) and it is likely that the resulting diatom community experienced  $\text{Si(OH)}_4$   
469 limitation by the end of the incubation period. Despite its relatively close proximity to  
470 land and relatively high dFe concentration ( $0.64 \text{ nmol L}^{-1}$ ), there was a pronounced  
471 response to Fe addition at C4 as demonstrated through higher  $F_v/F_m$ , PN-specific  $V\text{NO}_3$ ,  
472 and PC-specific VDIC in the Fe treatment compared to values in the unamended control  
473 by  $T_1$  (Fig. 2D-E; Supplemental Table 1). The  $\text{NO}_3^-:\text{Fe}$  ratio following artificial  $\text{NO}_3^-$   
474 addition was  $18.8 \mu\text{mol}:\text{nmol}$ , sufficiently high to cause Fe stress with phytoplankton  
475 growth following an increase in phytoplankton biomass.

477 Oceanic site O5 was located at Ocean Station Papa (OSP), station P26 of the  
478 Line-P transect (Fig. 1). This site demonstrated characteristically high macronutrients and  
479 low dFe ( $0.05 \text{ nmol L}^{-1}$ ), resulting in the highest  $\text{NO}_3^-:\text{Fe}$  ratio observed across all  
480 experimental sites ( $234 \mu\text{mol}:\text{nmol}$ ; Supplemental Table 1). Phytoplankton biomass was  
481 initially low, consistent with historical observations from this well-characterized Fe-  
482 limited region (Fig. 2A; Supplemental Table 1; Boyd and Harrison 1999). In contrast to  
483 most of the coastal sites, the majority of the phytoplankton biomass was dominated by  
484 picophytoplankton and other small cells ( $<5 \mu\text{m}$ ) initially and throughout the incubation  
485 period (Supplemental Table 1; Fig. 2B). Biogenic Si concentrations only increased after  
486 96 hours with similar responses in controls and Fe treatments (Fig. 2B). Both large and  
487 small chl *a* size fractions,  $F_v/F_m$ , PN-specific  $V\text{NO}_3$ , and PC-specific VDIC were higher in  
488 the Fe treatment than in the unamended control (Ctl), confirming that the phytoplankton  
489 community in the initial seawater and in all incubation treatments without added Fe were  
490 experiencing Fe limitation (Fig. 2B-E).

#### 491 *Community composition across sites*

492 Metatranscriptomic assembly of sequence data and subsequent taxonomic  
493 annotation yielded the relative transcript proportions of phytoplankton functional groups  
494 (Fig. 3). The CUZ site C1 was predominantly comprised of diatom transcripts at  $T_0$ ;  
495 however, there was a 26% decrease in diatom transcripts in both the Fe and DFB  
496 treatments by  $T_1$ , accompanied by genus-level shifts within the diatoms. In contrast, CUZ  
497 site C2 initially yielded a phytoplankton community transcript pool dominated equally by  
498 diatoms (30%) and prasinophytes (28%), with diatoms remaining a dominant taxa  
499 following incubation (26-28%) and prasinophyte transcripts substantially decreasing from  
500 28% to 3-8% in both Fe and DFB incubations. CUZ site C3 contained a phytoplankton  
501 community transcript pool almost equally represented by diatoms, prasinophytes,  
502 haptophytes and dinoflagellates with little change in community composition among  
503 treatments following incubation. The coastal subarctic Pacific site C4 yielded an initial  
504 phytoplankton community transcript pool dominated by dinoflagellate-assigned  
505 sequences (24%), although these sequences decreased by approximately 10% in the Fe  
506 treatment, concurrent with a 9% increase in diatom transcripts. At the oceanic site O5,  
507 there were initially equal proportions of prasinophyte (22%) and haptophyte (23%)  
508 transcripts, with little representation by diatoms (4%). However, diatom-assigned  
509 transcripts constituted 9% of the community transcript pool by  $T_2$  in the Fe addition  
510

511 treatment. *Pseudo-nitzschia* and *Thalassiosira* were among the top five diatom genera at  
512 all sites examined based on relative transcript abundance (Fig. 3). These two genera  
513 together constituted between 9 and 53% of the transcript proportions in the initial diatom  
514 communities, and 25-58% of the Fe-enriched diatom communities.

515

#### 516 *Gene expression responses to Fe status across sites*

517

518 Gene expression responses among sites were compared using Euclidian distance  
519 similarity analyses between Fe and DFB treatments (Fe/DFB, Fe/Ctl for O5) within the  
520 diatom genera *Pseudo-nitzschia* and *Thalassiosira* (Fig. 4). Expression responses within  
521 coastal sites clustered together (Supplemental Table 1), while the oceanic site O5  
522 displayed distinctly different patterns in both taxa. At site O5, 83 out of 1,334 KEGG  
523 Orthology genes (KOs) in *Pseudo-nitzschia* demonstrated >16-fold higher expression in  
524 the added Fe treatment than in the Fe-limited control treatment (Fig. 4). By comparison,  
525 155 out of 1,241 KOs in *Thalassiosira* showed >16-fold higher expression in the added  
526 Fe treatment compared to the low Fe control treatment. The most highly differentially  
527 expressed genes in oceanic *Pseudo-nitzschia* following Fe enrichment were ferritin (*FTN*,  
528 290-fold), a metal transporter (*CNNM*, 32-fold), a putative bicarbonate ( $\text{HCO}_3$ )  
529 transporter (*ICTB*, 133-fold), and an NADPH-dependent glutamate synthase (*GLT*; 146-  
530 fold). In oceanic *Thalassiosira*, highly differentially genes included ferredoxin-dependent  
531 sulfite reductase (*Fd-SIR*, 74-fold) and ferredoxin-dependent glutamate synthase (*Fd-*  
532 *GLT*; 416-fold). Fe addition induced both genera to increase the expression of several  
533 genes involved in photosynthesis by >16-fold exclusively at this location. Both taxa  
534 overexpressed gene products involved in vitamin biosynthesis, including the Fe-  
535 dependent vitamin B<sub>7</sub> synthesis protein biotin synthase (*BIOB*), which increased in the Fe  
536 enriched treatment expression by 84- and 49-fold in *Pseudo-nitzschia* and *Thalassiosira*,  
537 respectively. Furthermore, *Pseudo-nitzschia* increased expression of the vitamin B<sub>1</sub>  
538 (thiamine) biosynthetic gene *THIC* (by 179-fold) and vitamin B<sub>6</sub> (pyridoxine)  
539 biosynthetic genes pyridoxine kinase (*PDXK*; by 74-fold) and pyridoxine 4-  
540 dehydrogenase (*PLDH*; by 152-fold) following Fe enrichment at the oceanic site.

541

542 A number of genes demonstrated higher expression in the Fe-limited control  
543 treatment at O5. Forty-eight out of 1,334 genes in *Pseudo-nitzschia* and 77 out of 1,241  
544 genes in *Thalassiosira* showed >16-fold higher expression in the Ctl treatment than in the  
545 added Fe treatment, patterns that were not found in diatoms from the examined coastal  
546 sites (Fig. 4). In *Thalassiosira*, these genes encode proteins such as the copper (Cu)/zinc  
547 (Zn) superoxide dismutase (*Cu-Zn SOD*), an enzyme that removes toxic superoxide  
548 radicals by dismuting them into molecular oxygen and hydrogen peroxide, and a divalent  
549 metal transporter belonging to the ZIP family (*ZIP7*) (Marchetti and Maldonado, 2016).  
550 In both taxa, ribulose-1,5-bisphosphate carboxylase oxygenase (RubisCO; large subunit;  
551 *RBCL*), which catalyzes C-fixation in the Calvin cycle, had increased expression by  $\geq 24$ -  
552 fold in the Ctl treatment.

553

#### 554 *Influence of Fe availability on Fe metabolism*

555

556 The expression of genes involved in cellular growth and function, including N  
and C assimilation, vitamin synthesis, Fe-related metabolism and trace metal acquisition,

557 were compared in the dominant diatom genera *Pseudo-nitzschia* and *Thalassiosira*  
558 between the Fe and DFB/Ctl treatments (Fig. 5). Genes encoding proteins involved in  
559 metal transport were detected at all locations, with expression patterns varying depending  
560 on site and taxa. *Pseudo-nitzschia* increased expression of the Fe transporter *ABC.FEV.S*  
561 by >2-fold under Fe enrichment at all locations where incubated communities showed a  
562 physiological Fe effect (C3, C4, O5; Supplemental Table 1). Transcripts for another Fe  
563 uptake protein, the high affinity iron permease *FTR*, were generally more abundant in the  
564 DFB/Ctl treatments in *Thalassiosira*, although the gene was more highly expressed  
565 following Fe enrichment in *Pseudo-nitzschia* at sites C2, C3 and O5 (Fig. 5). The  
566 putative metal transporter *CNNM* was 32-fold more highly expressed following Fe  
567 enrichment in *Pseudo-nitzschia* at the oceanic site, but was not detected in *Thalassiosira*.  
568 Conversely, the non-specific metal transporter *ZIP7* was 21-fold more highly expressed  
569 under Fe-limited conditions in oceanic *Pseudo-nitzschia* and similarly not detected in  
570 oceanic *Thalassiosira*. Transcripts for Fe starvation induced proteins (*ISIPs*), including  
571 the recently-identified Fe acquisition protein *ISIP2A* that binds Fe at the cell surface and  
572 is thought to be involved in intracellular Fe transport (Morrissey et al. 2015), were highly  
573 abundant in Fe-stressed treatments (e.g. DFB and/or Ctl depending on the site) across all  
574 sites and in both taxa (Fig. 5). Although their specific functions in diatoms are unclear,  
575 other *ISIPs* were markedly abundant and differentially expressed in the DFB/Ctl  
576 treatments, with *ISIP1* one of the most differentially expressed genes between Fe-replete  
577 and Fe-limited treatments at each experimental site and in both taxa (Supplemental Fig.  
578 2).

579  
580 Other Fe-related metabolic processes similarly varied depending on both site and  
581 taxa. Differences in expression patterns between taxa were generally greater for these Fe-  
582 related genes than in the N- and C-related genes investigated (Fig. 5). At most sites,  
583 transcripts for the Fe storage protein ferritin (*FTN*) were higher in the Fe addition  
584 treatments than in the DFB/Ctl treatments. However, at two sites (C2 and C4), *FTN*  
585 transcripts were more abundant in the DFB treatment compared to the Fe addition  
586 treatment for one of the two genera (e.g., at site C2, 3.5-fold higher in *Pseudo-nitzschia*,  
587  $p = 1 \times 10^{-3}$  and at site C4, 90-fold in *Thalassiosira*). *SODs* were additionally differentially  
588 expressed, but they showed different expression patterns depending on the enzymes'  
589 metal cofactor(s) and the diatom genus. *Cu-Zn SOD*, which contains both Cu and Zn at  
590 its active site, showed a >100-fold higher expression in *Thalassiosira* in the Fe-limited  
591 control than in the added Fe treatment at the HNLC site O5. In contrast, in the same Fe-  
592 limited control treatment at this location, *Pseudo-nitzschia* demonstrated 2-fold higher  
593 expression of *Fe-Mn SOD*, which contains either Fe or manganese (Mn) as its metal  
594 cofactor. Based on the presence of Mn-coordinating amino acids at sites G-77 and Q-146  
595 of the most highly expressed *Fe-Mn SOD* contigs, this *Pseudo-nitzschia* *SOD* was  
596 determined to specifically utilize Mn as its metal cofactor (Groussman et al., 2015)  
597 (Supplemental Fig. 4C).

598  
599 Transcriptional responses of genes encoding Fe-dependent proteins and their  
600 functional replacements in photosynthetic electron transport were examined in both  
601 diatom genera (Fig. 5). Transcripts for the Fe-independent protein flavodoxin (*FLDA*),  
602 which functionally replaces the Fe-protein ferredoxin (*PETF*) in photosynthetic electron

603 transport, were generally more abundant in the DFB/Ctl treatments than in the Fe  
604 treatments in both genera (Fig. 5). Conversely, transcripts of *PETF* were >2-fold higher  
605 in the high-Fe treatment only in *Thalassiosira* and across all sites. In *Pseudo-nitzschia*,  
606 *PETF* transcripts were either constitutively expressed (C3 and C4), more highly  
607 expressed in the DFB treatment (C1), or not present (C2 and O5) (Fig. 5). Transcripts of  
608 cytochrome *c*<sub>6</sub> (*PETJ*) and its functional non-Fe replacement, the copper-protein  
609 plastocyanin, also showed differences in gene expression. *PETJ* transcripts were more  
610 abundant in the high Fe treatment at all sites and in both genera, except O5, where it was  
611 slightly more abundant in the Fe-limited control treatment (Fig. 5). By contrast,  
612 transcripts for plastocyanin (*PETE*) displayed inconsistent expression trends in response  
613 to Fe status across sites, being relatively more abundant following Fe enrichment in both  
614 genera at C3 (1.4-fold in *Pseudo-nitzschia*.; 1.9-fold in *Thalassiosira*,  $p = 5 \times 10^{-4}$ ) and at  
615 the initially Fe-limited oceanic site, O5 (1.4-fold in *Thalassiosira*; Fig. 5). At all other  
616 locations *PETE* transcripts were either more abundant under DFB conditions or not  
617 detected.

618  
619 Transcripts for the Fe-free protein rhodopsin (*RHO*) furthermore demonstrated  
620 differences in expression patterns among genera. This protein can supplement Fe-  
621 intensive photosynthesis in the light-driven production of membrane proton gradients and  
622 ATP in some diatoms (Marchetti et al., 2015). Rhodopsin was not detected in  
623 *Thalassiosira* at any location while its expression increased in *Pseudo-nitzschia* by >2-  
624 fold in the DFB/Ctl treatments relative to the Fe treatment at the two lowest dFe sites [C3  
625 ( $p = 0.01$ ) and O5; Fig. 5; Supplemental Table 1]. At the other sites *RHO* expression was  
626 constitutive. These rhodopsin contigs were structurally similar to diatom rhodopsins  
627 identified within the MMETSP database ( $\geq 55\%$  similarity; Supplemental Fig. 4B).

628  
629 Relationships among Fe-related transcript abundance, experimental site and  
630 treatment were determined using Principal Components Analysis (PCA) individually for  
631 each diatom genus. Principle components P1 and P2 explained 54% of the variation in  
632 transcript abundance in *Pseudo-nitzschia* and 76% in *Thalassiosira* (Fig. 6C). In *Pseudo-*  
633 *nitzschia*, transcripts for the photosynthetic genes ferredoxin-NADP<sup>+</sup> reductase (*PETH*),  
634 *PETJ*, a cytochrome *b*<sub>6</sub>/*f* complex protein (*PETC*), *FTN*, and *Cu-Zn SOD* were in higher  
635 relative abundance within Fe addition treatments while *RHO*, *ISIPs*, *FLDA*, *PETE* and  
636 *FTR* were generally more abundant in the Ctl and/or DFB treatments, as the principle  
637 component P1 separated these samples based on Fe treatment. In *Thalassiosira*, a similar  
638 response was observed, although *RHO* was not detected, and *PETF*, which was  
639 sporadically found and not abundant in *Pseudo-nitzschia*, strongly co-varied with the  
640 other genes highly expressed in the treatments where Fe was added (Fig. 6C).

641

#### 642 *Influence of Fe availability on N metabolism*

643

644 Genes involved in N transport and metabolism were investigated to assess the  
645 influence of varying Fe status on N assimilation. Transcripts for genes encoding nitrate  
646 (*NRT2*) and ammonium (*AMT*) transporters were detected at all locations, with *NRT2*  
647 increasing in expression by >2-fold in response to Fe addition relative to the DFB/Ctl  
648 treatment at the majority of sites in both taxa, while *AMT* expression varied depending on

649 site (Fig. 5). For instance, C4 was the only location with a >2-fold increase in *AMT*  
650 expression in the DFB treatment in both *Pseudo-nitzschia* and *Thalassiosira*. Transcripts  
651 corresponding to genes encoding components of NO<sub>3</sub><sup>-</sup> assimilation, including nitrate (*NR*)  
652 and nitrite reductases (*NIRA*, *NIRB*, *NIT-6*) were generally more abundant in the  
653 treatments with added Fe, although *NIRA* and *NIRB* displayed opposite expression  
654 patterns in *Pseudo-nitzschia* and *Thalassiosira* at site C3 (Fig. 5). Furthermore *Pseudo-*  
655 *nitzschia* increased gene expression of one group of nitrite reductases [*NIRB* and *NIT-6*,  
656 which use NADPH as the reductant (Brown et al., 2009)] by 11-fold and 3.6-fold,  
657 respectively, following added Fe while *Thalassiosira* conversely increased *NIRB*  
658 expression by 3.7-fold in the DFB treatment (Fig. 5). In addition, *Thalassiosira* increased  
659 gene expression of another form of nitrite reductase [*NIRA*, which uses  
660 ferredoxin/ flavodoxin as reductant (Brown et al., 2009)] by 8-fold ( $p = 3 \times 10^{-22}$ ) following  
661 Fe enrichment while *Pseudo-nitzschia* constitutively expressed *NIRA* at this location.  
662 Noticeably, transcripts for the genes encoding *NIRB* and *NIT-6* were present in at least  
663 one of the two diatom taxa examined at all sites except the oceanic site, O5.  
664

665 The relationships among transcript abundance for N uptake and assimilation-  
666 related genes, experimental sites, treatments and PN-specific VNO<sub>3</sub> measurements within  
667 the >5 μm size fraction of the phytoplankton community were examined via PCA bi-  
668 plots. Principle components P1 and P2 explained 86% of the variation in N-related  
669 transcript abundance in *Pseudo-nitzschia* and 88% in *Thalassiosira* (Fig. 6A). Sites  
670 generally contained high transcript abundances of *NRT2* and *NR* in the added Fe  
671 treatment, with the two genes strongly co-varying with one another in both *Pseudo-*  
672 *nitzschia* and *Thalassiosira*. Furthermore, the Fe addition treatments at two sites that  
673 experienced NO<sub>3</sub><sup>-</sup> depletion following incubation, C2 and C3, clustered together and  
674 contained the highest *AMT* transcript abundance at T<sub>1</sub> and T<sub>2</sub>, respectively.  
675 Phytoplankton communities within these incubation treatments concomitantly displayed  
676 low PN-specific VNO<sub>3</sub> (0.03 – 0.13 day<sup>-1</sup>; Fig. 6A). The highest PN-specific VNO<sub>3</sub> were  
677 observed in the added Fe treatment at site C4 at T<sub>1</sub> and at C1 within the initial (T<sub>0</sub>)  
678 phytoplankton community (1.4 day<sup>-1</sup>), which coincided with high abundances of *NIRA*  
679 transcripts in both genera at these locations.  
680

#### 681 *Influence of Fe availability on C metabolism*

682

683 To further gain insight into how variable Fe status influences macronutrient  
684 resource utilization and regional biogeochemistry, genes involved in C transport and  
685 fixation were examined among sites and between diatom genera. Transcripts  
686 corresponding to a carbonic anhydrase belonging to the α-family (*a-CA*), involved in the  
687 carbon concentrating mechanism (CCM) within photosynthetic eukaryotes (Reinfelder,  
688 2011), were either constitutively expressed, not detected, or more highly expressed in the  
689 DFB treatment at all locations apart from C1, where expression was 7-fold higher  
690 following Fe addition in *Thalassiosira* (Fig. 5).  
691

692 Members of the solute carrier (SLC) family of bicarbonate transporters (*SLC4A-1*,  
693 *-2*, and *-4*), which import bicarbonate ions from the environment also thought to be  
694 involved in the CCM (Nakajima et al., 2013), were detected intermittently among sites,

695 though in low transcript abundance (Fig. 5). These genes share sequence homology with  
696 the *Phaeodactylum tricornutum* genes *PtSLC4-1*, *-2* and *-4* in (BLASTP;  $E < 2 \times 10^{-69}$ ).  
697 These genes displayed inconsistent patterns of gene expression with each another, with  
698 no clear relationship to carbon assimilation rates. Another putative bicarbonate  
699 transporter (*ICTB*) was detected intermittently across sites and solely in *Pseudo-nitzschia*,  
700 where it was notably more highly expressed by 128-fold following Fe addition at O5.  
701 Conversely in *Thalassiosira*, the gene encoding phosphoenolpyruvate carboxylase  
702 (*PEPC*), which is part of a C<sub>4</sub>-CCM in some species of this genus (Reinfelder, 2011), was  
703 more highly expressed by 73-fold following Fe addition at O5.

704  
705 Gene expression of RubisCO (*RBCL*) increased by >24-fold in the Fe-limited  
706 control treatment in both genera at site O5 while at other sites the gene was either  
707 constitutively expressed, increased expression in the added Fe treatment, or not detected  
708 (Fig. 5). In addition, other genes involved in the Calvin Cycle, including  
709 phosphoglycerate kinase (*PGK*), transketolase (*TKL*), ribulose-phosphate 3-epimerase  
710 (*RPE*), and phosphoribulokinase (*PRK*), generally increased in expression following Fe  
711 addition compared to the DFB/Ctl treatment at one or more of the three sites experiencing  
712 some degree of Fe limitation (C3, C4, and O5; Supplemental Table 1; Fig. 5). At the  
713 CUZ sites C1 and C2, transcripts for these genes were either not differentially expressed  
714 or were more abundant in the DFB treatment within both diatom genera. Fructose-  
715 bisphosphate aldolases (*FBA*), involved in the Calvin Cycle, glycolysis and  
716 gluconeogenesis, demonstrated strong Fe-dependent transcriptional patterns regardless of  
717 site and taxa (Fig. 5). Transcripts corresponding to class II FBA, likely a metal-dependent  
718 aldolase, increased by 1.5 to 69-fold in the added Fe treatment as compared to DFB  
719 conditions with the largest fold change attributed to *Pseudo-nitzschia* from O5. Class II  
720 FBA has been previously demonstrated to be abundant under high-Fe conditions in  
721 diatoms and is hypothesized to contain Fe<sup>2+</sup> as a metal cofactor (Allen et al., 2012;  
722 Horecker et al., 1972; Lommer et al., 2012). Transcripts corresponding to class I FBA,  
723 the metal-independent version of class II FBA, conversely increased by 1.3 to 16-fold in  
724 DFB compared to Fe treatments.

725 The relationships in transcript abundance among C fixation-related genes,  
726 experimental sites, incubated treatments and PC-specific VDIC measurements were  
727 assessed using PCA bi-plots. Principle components P1 and P2 together explained  
728 80% of the variation in C-related transcript abundance in *Pseudo-nitzschia* and 78%  
729 in *Thalassiosira* (Fig. 6B). Site C4 contained some of the highest PC-specific VDIC  
730 measurements within the >5 μm size fraction (0.65 – 1.6 day<sup>-1</sup>), and coincided with  
731 the highest transcript abundances of **PGK**, **PRK**, **FBP**, **TKL**, **RPE** and **GAPDH** in  
732 *Pseudo-nitzschia* (Fig 6B). Conversely, Fe-limited treatments from C3 and O5 had  
733 the lowest transcript abundances of these genes in both *Pseudo-nitzschia* and  
734 *Thalassiosira*, with principle component P1 separating these samples from other  
735 sites and treatments (Fig. 6C). Fe-limited sites C3 and O5 phytoplankton  
736 communities additionally displayed some of the lowest PC-specific VDIC observed  
737 (0.11 - 0.17 day<sup>-1</sup>).

## 738 Discussion

739 Prior to this study, our understanding of the strategies utilized by phytoplankton  
740 to cope with low Fe bioavailability and resupply across different coastal and oceanic  
741 regions was limited. Furthermore, whether diverse diatom genera from identical  
742 environments would respond similarly when exposed to changes in Fe availability was  
743 unresolved. The gene expression patterns presented here demonstrate that the  
744 cosmopolitan diatom genera *Pseudo-nitzschia* and *Thalassiosira* rely on diverse sets of  
745 strategies to handle Fe stress, and that oceanic diatoms from both groups are highly  
746 responsive to changes in Fe availability with a greater degree of differentially expressed  
747 genes involved in nitrate assimilation, carbon fixation and vitamin production compared  
748 to their coastal counterparts.

749

#### 750 *Iron-related gene expression responses across sites*

751 Differences in gene expression patterns in response to Fe status were observed  
752 between the coastal (C1-C4) and oceanic sites (O5) examined in this study. This included  
753 the >16-fold higher expression of genes in the added Fe treatment relative to the Fe-  
754 limited control encoding proteins involved in B<sub>7</sub> synthesis (*BIOB*) in both taxa, and B<sub>1</sub>  
755 (*THIC*) and B<sub>6</sub> (*PDXK*, *PDLH*) synthesis in *Pseudo-nitzschia*. These increases are  
756 consistent with previous field observations demonstrating that Fe enrichment of  
757 previously Fe-limited oceanic diatom communities stimulates B-vitamin transcript  
758 production (Cohen et al., 2017). Genes encoding an Fe storage protein (ferritin [*FTN*])  
759 and components of amino acid metabolism (glutamate synthase [*GLT*] in *Pseudo-*  
760 *nitzschia*; ferredoxin-dependent glutamate synthase [*Fd-GLT*] in *Thalassiosira*) were  
761 similarly more highly expressed by >16-fold following Fe addition exclusively O5.  
762 Conversely, in the Fe-limited control, we observed the >16-fold higher expression of  
763 genes encoding the proteins Cu-Zn superoxide dismutase (Cu-Zn *SOD*) and RubisCO  
764 (*RBCL*), in either one or both taxa investigated. These distinct transcriptomic patterns of  
765 genes involved in diverse metabolic processes reflect differences in environmental factors  
766 selecting for diatom growth between the chronically Fe-limited open ocean and  
767 sporadically Fe-limited coastal regions.

768

769 In contrast, many photosynthetic genes were highly expressed following Fe  
770 addition regardless of location. A subset of these genes displayed distinct expression  
771 responses depending on whether the incubated communities experienced Fe limitation of  
772 growth rate (e.g., C3 and O5) or only Fe stress (C4; Supplemental Table 1). One such  
773 gene encodes the putative Fe transporter *ABC.FEV.S*, in which expression increased  
774 following Fe addition in *Pseudo-nitzschia* only at sites C3, C4, and O5. Additional genes  
775 include flavodoxin (*FLDA*) and plastocyanin (*PETE*), in which transcripts were generally  
776 more abundant in the DFB or Fe-limited Ctl treatments, consistent with flavodoxin's role  
777 as an Fe-independent photosynthetic electron carrier and plastocyanin's role as a Cu-  
778 dependent replacement for Fe-dependent cytochrome c<sub>6</sub>. At the Fe-stressed CUZ site C3  
779 however, *FLDA* was either constitutively expressed or slightly more abundant after Fe  
780 addition, depending on the diatom genus. Plastocyanin (*PETE*) transcripts were similarly  
781 more abundant after Fe addition in both diatom genera at C3 and in *Thalassiosira* at O5.  
782 This pattern suggests coastal diatoms from higher-Fe systems tend to temporarily replace  
783 Fe-dependent photosynthetic proteins with Fe-independent ones, while certain diatoms in

784 chronically Fe-limited environments may rely exclusively on Fe-free alternatives  
785 (Marchetti et al., 2012).

786

787 *Fe-related gene expression responses between diatom taxa*

788 *Pseudo-nitzschia* and *Thalassiosira* demonstrated several distinct responses to  
789 changes in Fe status despite co-existing under identical environmental conditions.  
790 Ferredoxin (*PETF*), ferredoxin-dependent glutamate synthase (*Fd-GLT*) and ferredoxin-  
791 dependent sulfite reductase (*Fd-SIR*) transcripts were more abundant in *Thalassiosira* at  
792 oceanic site O5 following Fe addition with these responses absent in *Pseudo-nitzschia*. In  
793 contrast, ferredoxin-related transcripts in oceanic *Pseudo-nitzschia* were constitutively  
794 expressed or not detected. These patterns may suggest oceanic *Thalassiosira* strongly  
795 utilizes ferredoxin and ferredoxin-dependent proteins following Fe addition while  
796 *Pseudo-nitzschia* relies on Fe-independent machinery. Site O5 was additionally the only  
797 location in which *Thalassiosira* increased gene expression of *Cu-Zn SOD* under Fe-  
798 limitation. This pattern was not evident in oceanic *Pseudo-nitzschia*, where gene  
799 expression of this protein was constitutive, or by either genus at coastal sites, suggesting  
800 that the oceanic *Thalassiosira* species have distinctly evolved to rely on this Cu- and Zn-  
801 containing enzyme as the preferred superoxide dismutase in their Fe-limited  
802 environment. *Pseudo-nitzschia* conversely increased expression of *Mn SOD* following Fe  
803 addition, likely as a result of iron-induced increases in photosynthetic rates and  
804 photosynthetic production of superoxide radicals (Asada, 2006). These patterns highlight  
805 differences in preferred metal cofactors as a function of Fe status and transcriptional  
806 tendencies between the two taxa.

807

808 Transcripts corresponding to rhodopsin (*RHO*) increased in abundance within  
809 *Pseudo-nitzschia* in the DFB/Ctl treatments at the two sites experiencing pronounced Fe  
810 limitation (C3 and O5), but were not identified in *Thalassiosira* from any location. This is  
811 consistent with rhodopsin being undetected in sequenced *Thalassiosira* spp.  
812 transcriptomes (Marchetti et al., 2015) and supports the notion that *Pseudo-nitzschia*  
813 may have a competitive advantage over non-rhodopsin containing taxa, allowing for an  
814 Fe-independent alternative to photosynthesis for ATP generation during times of Fe  
815 stress. Ferritin (*FTN*) gene expression patterns furthermore diverged between the two  
816 taxa at the coastal sites C4 (Line-P) and C2 (CUZ). This supports laboratory findings  
817 suggesting *FTN* may exhibit different expression patterns among diverse phytoplankton  
818 (Botebol et al., 2015; Marchetti et al., 2009), even between taxa residing in the same  
819 location. Lastly, *ABC.FEV.S*, encoding a membrane Fe transport system protein,  
820 displayed divergent expression patterns between the examined genera with only *Pseudo-*  
821 *nitzschia* increasing *ABC.FEV.S* expression after Fe addition in all incubations exhibiting  
822 signs of iron limitation (C3, C4 and O5).

823

824 Taken together, these patterns in gene expression demonstrate that members of  
825 the pennate diatom genus *Pseudo-nitzschia* and the centric diatom genus *Thalassiosira*  
826 restructure their functional metabolism in response to changes in Fe availability in  
827 distinct manners, possibly allowing both species to co-exist in the same environment.  
828 Both taxa are equipped with strategies to sustain growth under chronic Fe limitation in  
829 the open ocean, as supported by their equal transcript abundance during initial sampling.

830 Following pulse Fe additions however, oceanic *Pseudo-nitzschia* relies in part on the  
831 strategies discussed above to gain a competitive advantage over *Thalassiosira* and  
832 quickly dominates the phytoplankton community. It remains unclear however which  
833 combination of environmental factors in the NE Pacific Ocean would select for the  
834 preferential growth of *Thalassiosira* over *Pseudo-nitzschia*. We conclude that substantial  
835 differences in molecular responses to changes in Fe status are observed across taxonomic  
836 groups, and patterns in gene expression should not be assumed universal across diverse  
837 taxa or environments.

838

#### 839 *Nitrogen-related gene expression as a function of Fe status*

840 The majority of N transport and assimilation genes investigated increased in  
841 expression following Fe addition in both *Pseudo-nitzschia* and *Thalassiosira*. Several  
842 site- and taxa-specific patterns were identified, with some trends also possibly explained  
843 by each site's initial  $\text{NO}_3^-$  concentrations. For example, most gene copies encoding the  
844  $\text{NO}_3^-$  transporter, *NRT2*, have been demonstrated in laboratory cultures to increase in  
845 expression in  $\text{NO}_3^-$ -stressed diatoms (Bender et al., 2014; Rogato et al., 2015), and  
846 transcripts corresponding to this gene were some of the most abundant in both *Pseudo-*  
847 *nitzschia* and *Thalassiosira* at C2 – the CUZ site where  $\text{NO}_3^-$  concentrations were  
848 depleted in all incubations by the first sampling time point. This gene also showed  
849 expression trends that correlated with Fe status; *NRT2* transcripts were more abundant  
850 after Fe addition at all locations, regardless of initial  $\text{NO}_3^-$  concentrations. Based on these  
851 observations, *NRT2* in diatoms also appears to be linked to Fe status and follows the  
852 expression of other N-related genes involved in Fe-dependent  $\text{NO}_3^-$  assimilation,  
853 including those encoding nitrate reductase (*NR*) and nitrite reductase (*NIRA*; Marchetti *et*  
854 *al.*, 2012).

855

856 Diatoms were perhaps relying on  $\text{NH}_4$  in place of  $\text{NO}_3^-$  as a source of N based on  
857 gene expression patterns at several CUZ sites. Fe-enriched treatments at C2 contained the  
858 lowest  $\text{NO}_3^-$  after 48 hours of incubation ( $0.06 \mu\text{mol L}^{-1}$ ), and the gene encoding the  
859 ammonium transporter *AMT* concomitantly increased in expression in the Fe relative to  
860 DFB treatment (Fig. 6). Furthermore at C3, Fe-enriched communities entered  $\text{NO}_3^-$  stress  
861 by the end of the incubation period, and *AMT* expression simultaneously increased in  
862 both *Pseudo-nitzschia* and *Thalassiosira*. This negative relationship between  $\text{NO}_3^-$   
863 concentrations and *AMT* transcript abundance in natural diatom assemblages is consistent  
864 with those in laboratory *Pseudo-nitzschia multiseries* and *Fragilariopsis cylindrus*  
865 cultures (Bender et al., 2014; Rogato et al., 2015), and is reported here as one of the first  
866 observations of this relationship in natural phytoplankton communities.

867

868 High *AMT* transcript abundance at some of these locations may also represent  
869  $\text{NH}_4$  rather than  $\text{NO}_3^-$  being preferred as an N source by Fe-stressed diatoms conserving  
870 their cellular Fe supply, as  $\text{NO}_3^-$  reduction depends on various Fe-dependent processes,  
871 including  $\text{NO}_3^-$  and  $\text{NO}_2^-$  reduction (Milligan and Harrison, 2000). This is supported by  
872 the increased expression of *AMT* transcripts in both *Pseudo-nitzschia* and *Thalassiosira*  
873 from the Fe-stressed coastal Line-P site C4. *Pseudo-nitzschia* from the Fe-limited site O5  
874 also exhibited this pattern whereas *Pseudo-nitzschia* from C3 and *Thalassiosira* from

875 both C3 and O5 did not, suggesting other environmental parameters aside from Fe status  
876 are influencing whether diatoms utilize NH<sub>4</sub><sup>-</sup> or NO<sub>3</sub>-specific N uptake pathways.

877

878         Similar to our Fe-related gene expression results, several N-related genes  
879 demonstrated divergent expression responses between *Pseudo-nitzschia* and  
880 *Thalassiosira*. Expression of the NO<sub>2</sub><sup>-</sup> reductase genes, *NIRA* and *NIRB*, displayed  
881 opposite patterns between the two genera at the CUZ site where Fe-stress occurred in  
882 incubations (C3), with *Pseudo-nitzschia* highly expressing the gene encoding non-  
883 ferredoxin-utilizing NO<sub>2</sub><sup>-</sup> reductase (*NIRB*) following Fe addition, and *Thalassiosira*  
884 highly expressing the gene encoding the ferredoxin-utilizing nitrite reductase (*NIRA*).  
885 Furthermore at site O5, *Pseudo-nitzschia* increased expression of *AMT* and NADPH-  
886 dependent glutamate synthase (*GLT*) following Fe addition while *Thalassiosira* increased  
887 expression of *NRT2* and ferredoxin-dependent glutamate synthase (*Fd-GLT*). These  
888 transcriptomic patterns may suggest *Pseudo-nitzschia* continues to rely on the non-Fe  
889 requiring metabolic pathways for assimilating N once Fe becomes available (*AMT*, *NIRB*,  
890 *GLT*), whereas *Thalassiosira* shifts over to Fe-dependent ones (*NRT2*, *NIRA*, *Fd-GLT*)  
891 upon resupply.

892

893         These expression patterns furthermore support that substantial variations exist  
894 between the two diatom taxa in terms of N acquisition and assimilation strategies  
895 following changes in Fe supply. Both *Pseudo-nitzschia* and *Thalassiosira* are equipped  
896 with distinct strategies to compete under a variety of Fe and N conditions, and this may  
897 contribute to how multiple diatom species relying upon the same limiting resources in  
898 identical environments co-exist (i.e., paradox of the plankton; Hutchinson, 1961). These  
899 patterns are furthermore consistent with previous reports of resource partitioning among  
900 diatoms based on N and phosphate utilization (Alexander et al., 2015). Varying  
901 environmental pressure likely maintain populations of diverse diatom genera in the open  
902 ocean, with certain species outcompeting others depending on specific sets of external  
903 factors, including both macro- and micronutrients (Godhe and Rynearson, 2017).

904

#### 905 *Carbon-related gene expression responses as a function of Fe status*

906         Genes encoding proteins involved in C uptake and assimilation were surveyed in  
907 order to determine the influence of Fe addition or stress on C metabolism. We observed  
908 site-specific expression patterns of the diatom RubisCO large subunit protein (*RBCL*),  
909 where gene expression was substantially elevated at site O5 in the Fe-limited control  
910 treatment relative to the Fe addition response in both diatom genera. A sequence analysis  
911 of RubisCO contigs obtained across experimental sites demonstrates that O5 protein  
912 sequences are structurally less similar to known *Pseudo-nitzschia* and *Thalassiosira*  
913 RubisCO protein sequences within the MMETSP database than those at the four coastal  
914 sites (Supplemental Fig. 4A; Supplemental Table 3). This distinction in both protein  
915 structure and transcriptional expression may indicate a distinct adaptation and utilization  
916 of RubisCO in the oceanic diatoms than in those from high-Fe coastal waters.  
917 Phylogenetically diverse diatom species have been demonstrated to vary in their  
918 RubisCO enzyme kinetics in laboratory cultures, with their RubisCO content inversely  
919 linked to the strength of their carbon concentrating mechanism (CCM; Young et al.,  
920 2016). The CCM increases CO<sub>2</sub> concentrations in chloroplast stroma in the vicinity of

921 RubisCO and is fueled by the energy (ATP) generated from the Fe-intensive process of  
922 photosynthesis (Reinfelder, 2011; Young et al., 2016). We hypothesize that chronically  
923 Fe-limited oceanic diatoms are ATP-limited by the scarcity of Fe needed to support  
924 photosynthesis, and instead increase their RubisCO protein content to maintain high rates  
925 carbon fixation rather than allocate scarce energy resources to the CCM. Further  
926 supporting this hypothesis, the genes encoding a putative bicarbonate transporter (*ICBT*)  
927 and a C<sub>4</sub>-CCM component (*PEPC*; Reinfelder, 2011; Reinfelder et al., 2000; Sage, 2004)  
928 were highly expressed following Fe addition in *Pseudo-nitzschia* and *Thalassiosira*,  
929 respectively, exclusively at O5. This supports that diatoms may be capable of shuffling  
930 energy pools into either the CCM or RubisCO production depending on Fe  
931 bioavailability. Interestingly, in laboratory-based proteomic analyses with cultures of the  
932 coastal diatom *Thalassiosira pseudonana*, RubisCO was similarly more highly expressed  
933 under Fe limitation, while PEPC protein levels were higher under Fe-replete conditions  
934 (Nunn et al., 2013) Laboratory-based RubisCO kinetic work with cultured diatom isolates  
935 is needed to confirm whether diatoms from HNLC regions minimize their photosynthetic  
936 demand for Fe by synthesizing more RubisCO enzymes rather than allocating scarce  
937 energy resources into the CCM.

938  
939 Other C fixation-related gene expression patterns were largely consistent with C  
940 assimilation rates, and generally varied as a function of both Fe status and ocean  
941 province. The genes *PGK*, *TKL*, *RPE*, and *PRK* did not exhibit site-specific expression  
942 patterns similar to *RBLC*, and instead increased in expression following Fe enrichment at  
943 sites where Fe addition increased C assimilation rates (C3, C4 and O5). Increased  
944 expression of these genes is expected with Fe stimulation of C-fixation and growth.  
945 These expression patterns are in agreement with laboratory cultures of the diatom  
946 *Phaeodactylum tricornutum*, which increased expression of genes involved in C fixation  
947 during the light portion of their diel cycle, when DIC is being taken up to support  
948 photosynthesis (Chauton et al., 2013).

949  
950 *Conclusion*

951 Gene expression characterization coupled with biological rate processes across  
952 geographically diverse communities suggests regional and taxa-specific strategies are  
953 utilized by diatoms when rapidly responding to variations in environment. Our analysis  
954 demonstrates that chronically Fe-limited oceanic diatoms will restructure Fe, N, and C  
955 metabolism in a distinctive manner following Fe addition when compared to the response  
956 of coastal diatom communities that receive inherently more variable Fe inputs. *Pseudo-*  
957 *nitzschia* and *Thalassiosira*, two cosmopolitan diatom taxa found at all locations  
958 investigated, at times demonstrated divergent transcriptomic responses to changes in Fe  
959 status in terms of photosynthetic processes and N metabolism, even under identical  
960 environmental conditions.

961 Potential limitations to our approach include gene expression analyses being  
962 conducted on specific diatom genera while the physiological rate process measurements  
963 correspond to bulk phytoplankton communities. We therefore assumed the physiological  
964 characteristics to be representative of all phytoplankton members present. Furthermore,  
965 the metatranscriptomic approach used here consisted of analyzing cumulative expression  
966 responses of pooled gene copies; however, distinct gene copies have been shown to vary

967 in their transcriptional response to environmental conditions within a single organism  
968 (Bender et al., 2014; Levitan et al., 2015; Rogato et al., 2015). In order to gain further  
969 resolution, we recommend laboratory-based studies be performed investigating the direct  
970 relationships between nutrient uptake rates and expression of specific gene copies  
971 encoding proteins involved in nutrient uptake and assimilation in distinct members from  
972 each of the genera *Pseudo-nitzschia* and *Thalassiosira*.

973 The findings presented here support the notion that a tremendous degree of  
974 genetic diversity is contained within even a single diatom lineage that may have a strong  
975 influence on the abundance and distribution of phytoplankton communities. Since Fe  
976 bioavailability to phytoplankton is predicted to change with increasing temperature and  
977 acidification of surface seawater (Capone and Hutchins, 2013; Hutchins and Boyd, 2016;  
978 Shi et al., 2010; Sunda, 2010), these findings will aid in predicting the consequences of  
979 changing ocean conditions on phytoplankton productivity and community composition.

980

#### 981 **Conflict of interest statement**

982 The authors declare that the research was conducted in the absence of any commercial or  
983 financial relationships that could be construed as potential conflicts of interest.

984

#### 985 **Authors and Contributions**

986 AM, BST and KB designed the study; NRC, KAE, BST and AM performed the  
987 incubation experiments; NRC conducted the metatranscriptomic and physiological  
988 analysis; RHL provided bioinformatic support; FIK and KT obtained photophysiological  
989 measurements onboard the *R/V Melville*; MAB and HM quantified biogenic silica; MMT  
990 provided primary productivity measurements; CPT and BST quantified trace metals;  
991 WGS contributed to iron metabolism interpretations; SB quantified domoic acid; NRC  
992 and AM wrote the manuscript. All authors contributed to intellectual content and  
993 approved the final manuscript.

994

#### 995 **Funding**

996 Research was funded through National Science Foundation grants OCE-1334935 to A.M,  
997 OCE-1334632 to B.S.T, OCE-1334387 to M.A.B, OCE-1333929 to K.T and OCE-  
998 1259776 to K.B., as well as through Discovery NSERC grant 261521-13 to M.T.M.

999

#### 1000 **Acknowledgements**

1001 We thank J. Roach (UNC), S. Haines (UNC), W. Gong (UNC), M. Kanke (UNC), S.  
1002 Davies (UNC) and M. Love (UNC) for sequencing analysis advice and guidance. P.  
1003 Morton (FSU) analyzed the dissolved Fe samples from the Line P cruise (C4 and O5).  
1004 Dissolved nutrients were analyzed by T. Coale (SIO) onboard the *R/V Melville* (C1-C3),  
1005 and by M. Belton (IOS) onboard the *CCGS J.P. Tully* (C4 & O5). Z. Li (Duke) provided  
1006 climatological remote sensing images in Fig. 1. We are grateful to the scientists and crew  
1007 of the *CCGS J.P. Tully* (Line-P cruise 2015-09) and the *R/V Melville* (cruise 1405) for  
1008 their support and assistance at sea. RNA-Seq data was processed using UNC's Research  
1009 Computing clusters.

1010

#### 1011 **References**

1012 Alexander, H., Jenkins, B. D., Rynearson, T. A., and Dyhrman, S. T. (2015).

1013 Metatranscriptome analyses indicate resource partitioning between diatoms in the  
1014 field. *Proc. Natl. Acad. Sci.* 112, E2182–E2190. Available at:  
1015 <http://www.pnas.org/content/112/17/E2182.abstract>.  
1016 Allen, A. E., LaRoche, J., Maheswari, U., Lommer, M., Schauer, N., Lopez, P. J., et al.  
1017 (2008). Whole-cell response of the pennate diatom *Phaeodactylum tricornutum* to  
1018 iron starvation. *Proc. Natl. Acad. Sci. U. S. A.* 105, 10438–10443.  
1019 doi:10.1073/pnas.0711370105.  
1020 Allen, A. E., Moustafa, A., Montsant, A., Eckert, A., Kroth, P. G., and Bowler, C. (2012).  
1021 Evolution and Functional Diversification of Fructose Bisphosphate Aldolase Genes  
1022 in Photosynthetic Marine Diatoms. *Mol. Biol. Evol.* 29, 367–379. Available at:  
1023 <http://mbe.oxfordjournals.org/content/29/1/367.abstract>.  
1024 Altschul, S. F., Gish, W., Miller, W., Myers, E. W., and Lipman, D. J. (1990). Basic local  
1025 alignment search tool. *J. Mol. Biol.* 215, 403–10. doi:10.1016/S0022-  
1026 2836(05)80360-2.  
1027 Armbrust, E. V. (2009). The life of diatoms in the world ' s oceans. *Nature* 459, 185–  
1028 192. doi:10.1038/nature08057.  
1029 Asada, K. (2006). Production and Scavenging of Reactive Oxygen Species in  
1030 Chloroplasts and Their Functions. *Plant Physiol.* 141, 391–396.  
1031 doi:10.1104/pp.106.082040.  
1032 Barwell-Clarke, J., and Whitney, F. (1996). Institute of ocean sciences nutrient methods  
1033 and analysis. *Can. Tech. Rep. Hydrogr. Ocean Sci.* 49. Available at:  
1034 <https://books.google.com/books?id=MGGpjwEACAAJ>.  
1035 Behrenfeld, M. J., and Milligan, A. J. (2013). Photophysiological Expressions of Iron  
1036 Stress in Phytoplankton. *Annu. Rev. Mar. Sci.* 5, 217–46. doi:10.1146/annurev-  
1037 marine-121211-172356.  
1038 Bender, S., Durkin, C., Berthiaume, C., Morales, R., and Armbrust, E. V. (2014).  
1039 Transcriptional responses of three model diatoms to nitrate limitation of growth.  
1040 *Front. Mar. Sci.* 1, 3. doi:10.3389/fmars.2014.00003.  
1041 Biller, D. V, and Bruland, K. W. (2012). Analysis of Mn, Fe, Co, Ni, Cu, Zn, Cd, and Pb  
1042 in seawater using the Nobias-chelate PA1 resin and magnetic sector inductively  
1043 coupled plasma mass spectrometry (ICP-MS). *Mar. Chem.* 130–131, 12–20.  
1044 doi:<http://dx.doi.org/10.1016/j.marchem.2011.12.001>.  
1045 Birol, I., Jackman, S. D., Nielsen, C. B., Qian, J. Q., Varhol, R., Stazyk, G., et al. (2009).  
1046 De novo transcriptome assembly with ABySS. *Bioinformatics* 25, 2872–2877.  
1047 doi:10.1093/bioinformatics/btp367.  
1048 Bolger, A. M., Lohse, M., and Usadel, B. (2014). Trimmomatic: A flexible trimmer for  
1049 Illumina sequence data. *Bioinformatics* 30, 2114–2120.  
1050 doi:10.1093/bioinformatics/btu170.  
1051 Botebol, H., Lesuisse, E., Sutak, R., Six, C., Lozano, J.-C., Schatt, P., et al. (2015).  
1052 Central role for ferritin in the day/night regulation of iron homeostasis in marine  
1053 phytoplankton. *Proc. Natl. Acad. Sci.* 112, 1–6. doi:10.1073/pnas.1506074112.  
1054 Bowler, C., Allen, A. E., Badger, J. H., Grimwood, J., Jabbari, K., Kuo, A., et al. (2008).  
1055 The *Phaeodactylum* genome reveals the evolutionary history of diatom genomes.  
1056 *Nature* 456, 239–244. doi:10.1038/nature07410.  
1057 Brown, K. L., Twing, K. I., and Robertson, D. L. (2009). Unraveling the regulation of  
1058 nitrogen assimilation in the marine diatom *Thalassiosira pseudonana*

1059 (Bacillariophyceae): Diurnal variations in transcript levels for five genes involved in  
 1060 nitrogen assimilation. *J. Phycol.* 45, 413–426. doi:10.1111/j.1529-  
 1061 8817.2009.00648.x.

1062 Bruland, K. W., Lohan, M. C., Aguilar-Islas, A. M., Smith, G. J., Sohst, B., and Baptista,  
 1063 A. (2008). Factors influencing the chemistry of the near-field Columbia River  
 1064 plume: Nitrate, silicic acid, dissolved Fe, and dissolved Mn. *J. Geophys. Res. Ocean.*  
 1065 113, n/a-n/a. doi:10.1029/2007JC004702.

1066 Bruland, K. W., Rue, E. L., and Smith, G. J. (2001). Iron and macronutrients in  
 1067 California coastal upwelling regimes : Implications for diatom blooms. *Limnol.*  
 1068 *Oceanogr.* 46, 1661–1674.

1069 Brzezinski, M. A., Krause, J. W., Bundy, R. M., Barbeau, K. A., Franks, P., Goericke, R.,  
 1070 et al. (2015). Enhanced silica ballasting from iron stress sustains carbon export in a  
 1071 frontal zone within the California Current. *J. Geophys. Res. Ocean.* 120, 4654–4669.  
 1072 doi:10.1002/2015JC010829.

1073 Capone, D. G., and Hutchins, D. a. (2013). Microbial biogeochemistry of coastal  
 1074 upwelling regimes in a changing ocean. *Nat. Geosci.* 6, 711–717.  
 1075 doi:10.1038/ngeo1916.

1076 Chase, Z., Hales, B., Cowles, T., Schwartz, R., and van Geen, A. (2005). Distribution and  
 1077 variability of iron input to Oregon coastal waters during the upwelling season. *J.*  
 1078 *Geophys. Res. C Ocean.* 110, 1–14. doi:10.1029/2004JC002590.

1079 Chauton, M. S., Winge, P., Brembu, T., Vadstein, O., and Bones, A. M. (2013). Gene  
 1080 Regulation of Carbon Fixation, Storage, and Utilization in the Diatom  
 1081 *Phaeodactylum tricornutum* Acclimated to Light/Dark Cycles. *Plant Physiol.* 161,  
 1082 1034–1048. doi:10.1104/pp.112.206177.

1083 Cohen, N. R., A. Ellis, K., Burns, W. G., Lampe, R. H., Schuback, N., Johnson, Z., et al.  
 1084 (2017). Iron and vitamin interactions in marine diatom isolates and natural  
 1085 assemblages of the Northeast Pacific Ocean. *Limnol. Oceanogr.*, n/a-n/a.  
 1086 doi:10.1002/lno.10552.

1087 de Baar, H. J. W., Boyd, P. W., Coale, K. H., Landry, M. R., Tsuda, A., Assmy, P., et al.  
 1088 (2005). Synthesis of iron fertilization experiments: From the iron age in the age of  
 1089 enlightenment. *J. Geophys. Res. C Ocean.* 110, 1–24. doi:10.1029/2004JC002601.

1090 Edgar, R. C. (2004). MUSCLE: multiple sequence alignment with high accuracy and  
 1091 high throughput. *Nucleic Acids Res.* 32, 1792–1797. Available at:  
 1092 <http://dx.doi.org/10.1093/nar/gkh340>.

1093 Godhe, A., and Rynearson, T. (2017). The role of intraspecific variation in the ecological  
 1094 and evolutionary success of diatoms in changing environments. *Philos. Trans. R.*  
 1095 *Soc. B Biol. Sci.* 372. Available at:  
 1096 <http://rstb.royalsocietypublishing.org/content/372/1728/20160399.abstract>.

1097 Graff van Creveld, S., Rosenwasser, S., Levin, Y., and Vardi, A. (2016). Chronic iron  
 1098 limitation confers transient resistance to oxidative stress in marine diatoms. *Plant*  
 1099 *Physiol.* 172, 968–979.

1100 Groussman, R. D., Parker, M. S., and Armbrust, E. V. (2015). Diversity and Evolutionary  
 1101 History of Iron Metabolism Genes in Diatoms. *PLoS One* 10, e0129081. Available  
 1102 at: <http://dx.doi.org/10.1371/journal.pone.0129081>.

1103 Harris, S. L., Varela, D. E., Whitney, F. W., and Harrison, P. J. (2009). Nutrient and  
 1104 phytoplankton dynamics off the west coast of Vancouver Island during the 1997/98

1105 ENSO event. *Deep Sea Res. Part II Top. Stud. Oceanogr.* 56, 2487–2502.  
1106 doi:<http://dx.doi.org/10.1016/j.dsr2.2009.02.009>.

1107 Hildebrand, M. (2005). Cloning and functional characterization of ammonium  
1108 transporters from the marine diatom *Cylindrotheca fusiformis* (Bacillariophyceae).  
1109 *J. Phycol.* 41, 105–113. doi:10.1111/j.1529-8817.2005.04108.x.

1110 Horecker, B. L., Tsolas, O., and Lai, C. Y. (1972). “6 Aldolases,” in *The Enzymes*, ed. P.  
1111 D. B. B. T.-T. Enzymes (Academic Press), 213–258.  
1112 doi:[http://dx.doi.org/10.1016/S1874-6047\(08\)60450-3](http://dx.doi.org/10.1016/S1874-6047(08)60450-3).

1113 Hutchins, D. A., and Boyd, P. W. (2016). Marine phytoplankton and the changing ocean  
1114 iron cycle. *Nat. Clim. Chang.* 6, 1072–1079. Available at:  
1115 <http://dx.doi.org/10.1038/nclimate3147>.

1116 Hutchins, D. A., and Bruland, K. W. (1998). Iron-limited diatom growth and Si:N uptake  
1117 ratios in a coastal upwelling regime. *Nature* 393, 561–564. Available at:  
1118 <http://dx.doi.org/10.1038/31203>.

1119 Hutchins, D. A., DiTullio, G. R., Zhang, Y., and Bruland, K. W. (1998). An iron  
1120 limitation mosaic in the California upwelling regime. *Limnol. Oceanogr.* 43, 1037–  
1121 1054. doi:10.4319/lo.1998.43.6.1037.

1122 Hutchins, D. A., Hare, C. E., Weaver, R. S., Zhang, Y., Firme, G. F., DiTullio, G. R., et al.  
1123 (2002). Phytoplankton iron limitation in the Humboldt Current and Peru Upwelling.  
1124 47, 997–1011.

1125 Hutchinson, G. E. (1961). The Paradox of the Plankton. *Am. Nat.* 95, 137–145. Available  
1126 at: <http://www.jstor.org/stable/2458386>.

1127 Johnson, K. S., Chavez, F. P., and Friederich, G. E. (1999). Continental-shelf sediment as  
1128 a primary source of iron for coastal phytoplankton. *Nature* 398, 697–700. Available  
1129 at: <http://dx.doi.org/10.1038/19511>.

1130 Keeling, P. J., Burki, F., Wilcox, H. M., Allam, B., Allen, E. E., Amaral-Zettler, L. A., et  
1131 al. (2014). The Marine Microbial Eukaryote Transcriptome Sequencing Project  
1132 (MMETSP): Illuminating the Functional Diversity of Eukaryotic Life in the Oceans  
1133 through Transcriptome Sequencing. *PLoS Biol.* 12.  
1134 doi:10.1371/journal.pbio.1001889.

1135 King, A. L., and Barbeau, K. (2007). Evidence for phytoplankton iron limitation in the  
1136 southern California Current System. *Mar. Ecol. Prog. Ser.* 342, 91–103. Available  
1137 at: <http://www.int-res.com/abstracts/meps/v342/p91-103/>.

1138 Klingenberg, H., and Meinicke, P. (2017). How To Normalize Metatranscriptomic Count  
1139 Data For Differential Expression Analysis. *bioRxiv*. Available at:  
1140 <http://biorxiv.org/content/early/2017/05/05/134650.abstract>.

1141 Krause, J. W., Brzezinski, M. A., Villareal, T. A., and Wilson, C. (2013). Biogenic silica  
1142 cycling during summer phytoplankton blooms in the North Pacific subtropical gyre.  
1143 *Deep Sea Res. Part I Oceanogr. Res. Pap.* 71, 49–60.  
1144 doi:<https://doi.org/10.1016/j.dsr.2012.09.002>.

1145 Kustka, A. B., Allen, A. E., and Morel, F. M. M. (2007). Sequence analysis and  
1146 transcriptional regulation of iron acquisition genes in two marine diatoms. *J. Phycol.*  
1147 43, 715–729. doi:10.1111/j.1529-8817.2007.00359.x.

1148 La Roche, J., Boyd, P. W., McKay, R. M. L., and Geider, R. J. (1996). Flavodoxin as an  
1149 in situ marker for iron stress in phytoplankton. *Nature* 382, 802–805. Available at:  
1150 <http://dx.doi.org/10.1038/382802a0>.

- 1151 Lam, P. J., and Bishop, J. K. B. (2008). The continental margin is a key source of iron to  
1152 the HNLC North Pacific Ocean. *Geophys. Res. Lett.* 35, 1–5.  
1153 doi:10.1029/2008GL033294.
- 1154 Lam, P. J., Bishop, J. K. B., Henning, C. C., Marcus, M. A., Waychunas, G. A., and  
1155 Fung, I. Y. (2006). Wintertime phytoplankton bloom in the subarctic Pacific  
1156 supported by continental margin iron. *Global Biogeochem. Cycles* 20, 1–12.  
1157 doi:10.1029/2005GB002557.
- 1158 Langmead, B., and Salzberg, S. L. (2012). Fast gapped-read alignment with Bowtie 2.  
1159 *Nat Methods* 9, 357–359. doi:10.1038/nmeth.1923.
- 1160 Levitan, O., Dinamarca, J., Zelzion, E., Lun, D. S., Guerra, L. T., Kim, M. K., et al.  
1161 (2015). Remodeling of intermediate metabolism in the diatom *Phaeodactylum*  
1162 *tricornutum* under nitrogen stress. *Proc. Natl. Acad. Sci.* 112, 412–417.  
1163 doi:10.1073/pnas.1419818112.
- 1164 Li, H., Handsaker, B., Wysoker, A., Fennell, T., Ruan, J., Homer, N., et al. (2009). The  
1165 Sequence Alignment/Map format and SAMtools. *Bioinformatics* 25, 2078–2079.  
1166 doi:10.1093/bioinformatics/btp352.
- 1167 Lommer, M., Roy, A.-S., Schilhabel, M., Schreiber, S., Rosenstiel, P., and LaRoche, J.  
1168 (2010). Recent transfer of an iron-regulated gene from the plastid to the nuclear  
1169 genome in an oceanic diatom adapted to chronic iron limitation. *BMC Genomics* 11,  
1170 718. doi:10.1186/1471-2164-11-718.
- 1171 Lommer, M., Specht, M., Roy, A.-S., Kraemer, L., Andreson, R., Gutowska, M. A., et al.  
1172 (2012). Genome and low-iron response of an oceanic diatom adapted to chronic iron  
1173 limitation. *Genome Biol.* 13, R66. doi:10.1186/gb-2012-13-7-r66.
- 1174 Maldonado, M. T., and Price, N. M. (2001). Reduction and transport of organically  
1175 bound iron by *Thalassiosira oceanica* (Bacillariophyceae). *J. Phycol.* 37, 298–310.  
1176 doi:10.1046/j.1529-8817.2001.037002298.x.
- 1177 Malviya, S., Scalco, E., Audic, S., Vincent, F., Veluchamy, A., Bittner, L., et al. (2016).  
1178 Insights into global diatom distribution and diversity in the world’s ocean. *Proc.*  
1179 *Natl. Acad. Sci.* 348, in review. doi:10.1073/pnas.1509523113.
- 1180 Marchetti, A., and Cassar, N. (2009). Diatom elemental and morphological changes in  
1181 response to iron limitation: a brief review with potential paleoceanographic  
1182 applications. *Geobiology* 7, 419–431. doi:10.1111/j.1472-4669.2009.00207.x.
- 1183 Marchetti, A., Catlett, D., Hopkinson, B. M., Ellis, K., and Cassar, N. (2015). Marine  
1184 diatom proteorhodopsins and their potential role in coping with low iron availability.  
1185 *ISME J* 9, 2745–2748. doi:10.1038/ismej.2015.74.
- 1186 Marchetti, A., and Maldonado, M. T. (2016). “Iron,” in *The Physiology of Microalgae*,  
1187 eds. M. A. Borowitzka, J. Beardall, and J. A. Raven (Cham: Springer International  
1188 Publishing), 233–279. doi:10.1007/978-3-319-24945-2\_11.
- 1189 Marchetti, A., Parker, M. S., Moccia, L. P., Lin, E. O., Arrieta, A. L., Ribalet, F., et al.  
1190 (2009). Ferritin is used for iron storage in bloom-forming marine pennate diatoms.  
1191 *Nature* 457, 467–470. doi:10.1038/nature07539.
- 1192 Marchetti, A., Schruth, D. M., Durkin, C. A., Parker, M. S., Kodner, R. B., Berthiaume,  
1193 C. T., et al. (2012). Comparative metatranscriptomics identifies molecular bases for  
1194 the physiological responses of phytoplankton to varying iron availability. *Proc. Natl.*  
1195 *Acad. Sci.* doi:10.1073/pnas.1118408109.
- 1196 Milligan, A. J., and Harrison, P. J. (2000). Effects of non-steady-state iron limitation on

1197 nitrogen assimilatory enzymes in the marine diatom *Thalassiosira weissflogii*  
 1198 (Bacillariophyceae). *J. Phycol.* 36, 78–86. doi:10.1046/j.1529-8817.2000.99013.x.  
 1199 Milne, A., Landing, W., Bizimis, M., and Morton, P. (2010). Determination of Mn, Fe,  
 1200 Co, Ni, Cu, Zn, Cd and Pb in seawater using high resolution magnetic sector  
 1201 inductively coupled mass spectrometry (HR-ICP-MS). *Anal. Chim. Acta* 665, 200–  
 1202 207. doi:http://dx.doi.org/10.1016/j.aca.2010.03.027.  
 1203 Moore, J. K., Doney, S. C., Glover, D. M., and Fung, I. Y. (2002). Iron cycling and  
 1204 nutrient-limitation patterns in surface waters of the World Ocean. *Deep. Res. II* 49,  
 1205 463–507.  
 1206 Moore, J. K., Doney, S. C., and Lindsay, K. (2004). Upper ocean ecosystem dynamics  
 1207 and iron cycling in a global three-dimensional model. *Global Biogeochem. Cycles*  
 1208 18. doi:10.1029/2004GB002220.  
 1209 Morrissey, J., Sutak, R., Paz-Yepes, J., Tanaka, A., Moustafa, A., Veluchamy, A., et al.  
 1210 (2015). A Novel Protein, Ubiquitous in Marine Phytoplankton, Concentrates Iron at  
 1211 the Cell Surface and Facilitates Uptake. *Curr. Biol.* 25, 364–371.  
 1212 doi:http://dx.doi.org/10.1016/j.cub.2014.12.004.  
 1213 Nakajima, K., Tanaka, A., and Matsuda, Y. (2013). SLC4 family transporters in a marine  
 1214 diatom directly pump bicarbonate from seawater. *Proc. Natl. Acad. Sci.* 110, 1767–  
 1215 1772. Available at: <http://www.pnas.org/content/110/5/1767.abstract>.  
 1216 Nelson, D. M., DeMaster, D. J., Dunbar, R. B., and Smith, W. O. (1996). Cycling of  
 1217 organic carbon and biogenic silica in the Southern Ocean: Estimates of water-  
 1218 column and sedimentary fluxes on the Ross Sea continental shelf. *J. Geophys. Res.*  
 1219 101, 18519. doi:10.1029/96JC01573.  
 1220 Nuester, J., Vogt, S., and Twining, B. S. (2012). Localization of iron within centric  
 1221 diatoms of the genus *Thalassiosira*. *J. Phycol.* 48, 626–634. doi:10.1111/j.1529-  
 1222 8817.2012.01165.x.  
 1223 Nunn, B. L., Faux, J. F., Hippmann, A. A., Maldonado, M. T., Harvey, H. R., Goodlett,  
 1224 D. R., et al. (2013). Diatom Proteomics Reveals Unique Acclimation Strategies to  
 1225 Mitigate Fe Limitation. *PLoS One* 8, e75653. Available at:  
 1226 <https://doi.org/10.1371/journal.pone.0075653>.  
 1227 Pan, Y., Subba Roa, D. V., Mann, K. H., Brown, R. G., and Pocklington, R. (1996).  
 1228 Effects of silicate limitation on production of domoic acid, a neurotoxin, by the  
 1229 diatom *Pseudo-nitzschia multiseries*. I. Batch culture studies. *Mar. Ecol. Prog.*  
 1230 *Ser.* 131, 225–233. doi:10.3354/meps131235.  
 1231 Parker, C. E., Brown, M. T., and Bruland, K. W. (2016). Scandium in the open ocean: A  
 1232 comparison with other group 3 trivalent metals. *Geophys. Res. Lett.* 43, 2758–2764.  
 1233 doi:10.1002/2016GL067827.  
 1234 Parsons, T. R., Maita, Y., and Lalli, C. M. (1984). *A manual of chemical and biological*  
 1235 *methods for seawater analysis*. Oxford [Oxfordshire]; New York: Pergamon Press.  
 1236 Peers, G., and Price, N. M. (2006). Copper-containing plastocyanin used for electron  
 1237 transport by an oceanic diatom. *Nature* 441, 341–344. Available at:  
 1238 <http://dx.doi.org/10.1038/nature04630>.  
 1239 Rabosky, D. L., and Sorhannus, U. (2009). Diversity dynamics of marine planktonic  
 1240 diatoms across the Cenozoic. *Nature* 457, 183–186. Available at:  
 1241 <http://dx.doi.org/10.1038/nature07435>.  
 1242 Reinfelder, J. R. (2011). Carbon Concentrating Mechanisms in Eukaryotic Marine

1243 Phytoplankton. *Annu. Rev. Mar. Sci* 3, 291–317. doi:10.1146/annurev-marine-  
1244 120709-142720.

1245 Reinfelder, J. R., Kraepiel, A. M. L., and Morel, F. M. M. (2000). Unicellular C4  
1246 photosynthesis in a marine diatom. *Nature* 407, 996–999. Available at:  
1247 <http://dx.doi.org/10.1038/35039612>.

1248 Ribalet, F., Marchetti, A., Hubbard, K. A., Brown, K., Durkin, C. A., Morales, R., et al.  
1249 (2010). Unveiling a phytoplankton hotspot at a narrow boundary between coastal  
1250 and offshore waters. *Proc. Natl. Acad. Sci.* 107, 16571–16576. Available at:  
1251 <http://www.pnas.org/content/107/38/16571.abstract>.

1252 Robertson, G., Schein, J., Chiu, R., Corbett, R., Field, M., Jackman, S. D., et al. (2010).  
1253 De novo assembly and analysis of RNA-seq data. *Nat. Methods* 7, 909–12.  
1254 doi:10.1038/nmeth.1517.

1255 Robinson, M. D., McCarthy, D. J., and Smyth, G. K. (2010). edgeR: a Bioconductor  
1256 package for differential expression analysis of digital gene expression data.  
1257 *Bioinformatics* 26. doi:10.1093/bioinformatics/btp616.

1258 Robinson, M. D., and Oshlack, A. (2010). A scaling normalization method for  
1259 differential expression analysis of RNA-seq data. *Genome Biol.* 11, R25.  
1260 doi:10.1186/gb-2010-11-3-r25.

1261 Robinson, M. D., and Smyth, G. K. (2008). Small-sample estimation of negative  
1262 binomial dispersion, with applications to SAGE data. *Biostatistics* 9, 321–332.  
1263 doi:10.1093/biostatistics/kxm030.

1264 Rogato, A., Amato, A., Iudicone, D., Chiurazzi, M., Ferrante, M. I., and d’Alcalà, M. R.  
1265 (2015). The diatom molecular toolkit to handle nitrogen uptake. *Mar. Genomics* 24,  
1266 Part 1, 95–108. doi:<http://dx.doi.org/10.1016/j.margen.2015.05.018>.

1267 Sage, R. F. (2004). The evolution of C4 photosynthesis. *New Phytol.* 161, 341–370.  
1268 doi:10.1111/j.1469-8137.2004.00974.x.

1269 Shi, D., Xu, Y., Hopkinson, B. M., and Morel, F. M. M. (2010). Effect of ocean  
1270 acidification on iron availability to marine phytoplankton. *Science (80-. )*. 327, 676–  
1271 679. doi:10.1126/science.1183517.

1272 Sims, P. A., Mann, D. G., and Medlin, L. K. (2006). Evolution of the Diatoms: Insights  
1273 from Fossil, Biological and Molecular Data. *Phycologia* 45, 361–402. Available at:  
1274 <http://search.proquest.com/docview/198607320?accountid=14244>.

1275 Song, B., and Ward, B. B. (2007). Molecular cloning and characterization of high-affinity  
1276 nitrate transporters in marine phytoplankton. *J. Phycol.* 43, 542–552.  
1277 doi:10.1111/j.1529-8817.2007.00352.x.

1278 Strzepek, R. F., and Harrison, P. J. (2004). Photosynthetic architecture differs in coastal  
1279 and oceanic diatoms. *Nature* 431, 689–692. Available at:  
1280 <http://dx.doi.org/10.1038/nature02954>.

1281 Sunda, W. G. (2010). Iron and the Carbon Pump. *Science (80-. )*. 327, 654 LP-655.  
1282 Available at: <http://science.sciencemag.org/content/327/5966/654.abstract>.

1283 Sunda, W. G., and Huntsman, S. A. (1995). Iron uptake and growth limitation in oceanic  
1284 and coastal phytoplankton. *Mar. Chem.* 50, 189–206.  
1285 doi:[http://dx.doi.org/10.1016/0304-4203\(95\)00035-P](http://dx.doi.org/10.1016/0304-4203(95)00035-P).

1286 Sutak, R., Botbol, H., Blaiseau, P.-L., Léger, T., Bouget, F.-Y., Camadro, J.-M., et al.  
1287 (2012). A comparative study of iron uptake mechanisms in marine microalgae: Iron  
1288 binding at the cell surface is a critical step. *Plant Physiol.* 160, 2271–2284.

1289 Available at: <http://www.plantphysiol.org/content/160/4/2271.abstract>.  
1290 Taylor, F. J. R., and Haigh, R. (1996). Spatial and temporal distributions of  
1291 microplankton during the summers of 1992– 1993 in Barkley Sound, British  
1292 Columbia, with emphasis on harmful species. *Can. J. Fish. Aquat. Sci.* 53, 2310–  
1293 2322. doi:10.1139/f96-181.  
1294 Taylor, R. L., Semeniuk, D. M., Payne, C. D., Zhou, J., Tremblay, J.-É., Cullen, J. T., et  
1295 al. (2013). Colimitation by light, nitrate, and iron in the Beaufort Sea in late  
1296 summer. *J. Geophys. Res. Ocean.* 118, 3260–3277. doi:10.1002/jgrc.20244.  
1297 Varela, D. E., and Harrison, P. J. (1999). Effect of ammonium on nitrate utilization by  
1298 *Emiliana huxleyi*, a coccolithophore from the oceanic northeastern Pacific. *Mar.*  
1299 *Ecol. Prog. Ser.* 186, 67–74.  
1300 Whitney, L. P., Lins, J. J., Hughes, M. P., Wells, M. L., Chappell, P. D., and Jenkins, B.  
1301 D. (2011). Characterization of Putative Iron Responsive Genes as Species-Specific  
1302 Indicators of Iron Stress in Thalassiosiroid Diatoms. *Front. Microbiol.* 2, 234.  
1303 doi:10.3389/fmicb.2011.00234.  
1304 Young, J. N., Heures, A. M. C., Sharwood, R. E., Rickaby, R. E. M., Morel, F. M. M.,  
1305 and Whitney, S. M. (2016). Large variation in the Rubisco kinetics of diatoms  
1306 reveals diversity among their carbon-concentrating mechanisms. *J. Exp. Bot.* 67,  
1307 3445–3456. doi:10.1093/jxb/erw163.

1308

### 1309 **Figure Legends**

1310 *Figure 1.* Locations of incubation experiments in the California Upwelling Zone (C1,  
1311 C2, C3) and along Line P (C4, O5) in the Northeast Pacific Ocean. Color bar indicates  
1312 climatological-averaged chlorophyll *a* concentrations ( $\mu\text{g L}^{-1}$ ) from SeaWiFS (1997–  
1313 2010).

1314

1315 *Figure 2.* Dissolved macronutrient concentrations: nitrate ( $\text{NO}_3^-$ ), silicic acid ( $\text{SiOH}_4$ ),  
1316 and ortho-phosphate ( $\text{PO}_4$ ) (**A**), Size-fractionated chlorophyll *a* ( $\mu\text{g L}^{-1}$ ) within the large  
1317 ( $>5 \mu\text{m}$ ) and small ( $<5 \mu\text{m}$ ) size fractions or biogenic silica ( $\mu\text{mol L}^{-1}$ ) (**B**), Maximum  
1318 photochemical yield of PSII ( $F_v/F_m$ ) (**C**), Particulate carbon (PC)-specific dissolved  
1319 inorganic carbon (DIC) uptake rates [ $\text{VDIC} (\text{day}^{-1})$ ] within the large and small size  
1320 fractions (**D**), and particulate nitrogen (PN)-specific nitrate uptake rates [ $\text{VNO}_3 (\text{day}^{-1})$ ]  
1321 within the large and small size fractions in each treatment and sample time points across  
1322 sites (**E**) (see Supplemental Table 1). Where present, error bars represent the standard  
1323 deviation associated with the mean of triplicate incubations.

1324

1325 *Figure 3.* The average normalized transcript proportions of phytoplankton taxa (outer  
1326 charts) and diatom genera (inner charts) from initial seawater ( $T_0$ ) and during the first  
1327 time point ( $T_1$ ; see Supplemental Table 1) within the Fe addition (Fe) and DFB addition  
1328 (DFB) treatments at each site. Note that for site O5, the control (Ctl) treatment is  
1329 provided as the Fe-limited comparison.

1330

1331 *Figure 4.* Differential expression response of shared KEGG Orthologs (KOs) between  
1332 the Fe and DFB treatments at  $T_1$  in the diatom genera *Pseudo-nitzschia* (**A**) and  
1333 *Thalassiosira* (**B**). Heatmap represents the  $\log_2$  fold change in gene expression within the  
1334 Fe addition treatment relative to the DFB addition treatment at each site. For site O5, the

1335 T<sub>2</sub> control (Ctl) treatment is used as the Fe-limited comparison. Only KOs with transcript  
1336 abundances >5 log<sub>2</sub> CPM are included. Dendrograms reflect similarity in expression  
1337 responses among sites (columns) or KOs (rows).  
1338

1339 *Figure. 5.* Differential expression responses of select genes involved in nitrogen (N;  
1340 green), carbon (C; blue), metal transport (orange), iron (Fe; red), and vitamin (purple)-  
1341 related processes between the T<sub>1</sub> Fe and DFB/Ctl treatments within the diatom genera  
1342 *Pseudo-nitzschia* (P) and *Thalassiosira* (T) (A). Heatmap represents the log<sub>2</sub> fold change  
1343 of gene expression within the Fe addition treatment relative to the DFB treatment at each  
1344 site. For site O5, the T<sub>2</sub> control (Ctl) treatment is used as the Fe-limited comparison. Gray  
1345 boxes indicate transcripts were not detected in either treatment. White boxes signify no  
1346 change in expression between treatments. A schematic representation of N, C, Fe, metal  
1347 transport and vitamin-related processes within a diatom cell, color-coded by genes of  
1348 interest included in A (B). Adjacent proteins with black borders indicate similar cellular  
1349 functions (e.g., *FLDA*, *PETF*). Gene abbreviations are NRT2: nitrate transporter; AMT:  
1350 ammonium transporter; URTA: urea transporter; NR: nitrate reductase; NIRA:  
1351 ferredoxin-nitrite reductase; NIRB: nitrite reductase; NIT-6: nitrite reductase; GLT:  
1352 glutamate synthase; Fd-GLT: ferredoxin-glutamate synthase; α-CA: carbonic anhydrase  
1353 (α family); SLC4A: solute carrier family (bicarbonate transporters); ICTB: putative  
1354 bicarbonate transporter; PEPC: phosphoenolpyruvate carboxylase; RBCL: Rubisco large  
1355 subunit; RBCS: RubisCO small subunit; PGK: phosphoglycerate kinase; TPI:  
1356 triosephosphate isomerase; GAPDH: glyceraldehyde 3-phosphate dehydrogenase; FBP:  
1357 fructose-1,2-bisphosphatase I; TKL: transketolase; RPE: ribulose-phosphate 3-epimerase;  
1358 PRK: phosphoribulokinase; FBA class I: fructose bisphosphate aldolase (class I); FBA  
1359 class II: fructose bisphosphate aldolase (classII); FTR: high affinity iron permease;  
1360 ABC.FEV.S: iron complex transport system substrate-binding protein; ZIP7: zinc  
1361 transporter 7; CNNM: metal transporter; ISIP2A: iron starvation induced protein 2A;  
1362 ISIP1: iron starvation induced protein 1; ISIP2B: iron starvation induced protein 2B;  
1363 ISIP3: iron starvation induced protein 3; FTN: ferritin; FLDA: flavodoxin I; PETF:  
1364 ferredoxin; PETH: ferredoxin-NADP<sup>+</sup> reductase; PETE: plastocyanin; PETJ: cytochrome  
1365 c<sub>6</sub>; PETC: cytochrome b<sub>6</sub>/f complex; Cu-Zn SOD: superoxide dismutase containing Cu  
1366 and Zn as cofactors; Fe-Mn SOD: superoxide dismutase containing Fe or Mn as cofactor;  
1367 Fd-SIR: ferredoxin-sulfite reductase; RHO: rhodopsin (note the localization of RHO  
1368 within the vacuole membrane is speculative); BIOB: biotin synthase; PDXK: pyridoxal  
1369 kinase; PLDH: pyridoxal 4-dehydrogenase; THIC: phosphomethylpyrimidine synthase.  
1370

1371 *Figure. 6.* PCA bi-plots depicting the relationship between treatment (color), site (shape),  
1372 and biomass-normalized N and C rates for transcript abundances of genes involved in N,  
1373 C and Fe-related processes in *Pseudo-nitzschia* (left) and *Thalassiosira* (right). Size of  
1374 points scales with increasing PN-specific VNO<sub>3</sub> (day<sup>-1</sup>) from 0.04 to 1.63 day<sup>-1</sup> (A), and  
1375 with increasing PC-specific VDIC (day<sup>-1</sup>) from 0.01 to 1.50 day<sup>-1</sup> (B). For the Fe-related  
1376 genes transcript abundance PCA bi-plot, sizes remain constant across samples (C). See  
1377 Fig. 5 for list of gene abbreviations.  
1378

1379 *Supplemental Figure 1.* Irradiance and temperature of flow-through seawater within  
1380 onboard incubations during the (A) CUZ and (B) Line-P cruises. Incubators were used to

1381 maintain near-ambient surface water temperatures and irradiances during the incubation  
1382 period (48-96 hours; Supplemental Table 1). Plexiglass incubators were covered with  
1383 neutral density screening to achieve approximately 30% of the incident irradiance. PAR  
1384 ( $\mu\text{E}$ ) is shown in black, temperature ( $^{\circ}\text{C}$ ) in red.

1385  
1386 *Supplemental Figure 2.* MA plots depicting the differential expression response of KOs  
1387 within the diatom genera *Pseudo-nitzschia* and *Thalassiosira* between Fe addition (Fe)  
1388 and DFB addition (DFB) treatments across sites. Each point corresponds to a unique KO.  
1389 Points are shaded gray if transcripts were not significantly differentially expressed  
1390 ( $p < 0.05$ ; A-C only). Genes of interest involved in nitrogen (N; green), carbon (C; blue),  
1391 iron (Fe; red), vitamin (purple) metabolism or metal transport (orange) are labeled only if  
1392 differentially expressed ( $p < 0.05$ ; C1-C3 only) or if exhibited a  $>2$ -fold change (C4 &  
1393 O5). The unamended control treatment was used at site O5 in place of the DFB-addition  
1394 treatment. See Fig. 5 for a list of gene abbreviations.

1395  
1396 *Supplemental Figure 3.* Domoic acid (DA) concentrations within initial phytoplankton  
1397 communities ( $T_0$ ) and incubated treatments at CUZ sites C1-C3.

1398  
1399 *Supplemental Figure 4.* Alignments of RubisCO (large subunit; *RBCL*) (A), rhodopsin  
1400 (*RHO*) (B), and Fe/Mn-containing superoxide dismutase (*Fe-Mn SOD*) (C) amino acid  
1401 sequences among environmental contigs identified in this study and the MMETSP  
1402 database. Alignments were created using MUSCLE within Geneious version 5.6.4 (Edgar  
1403 2004; Tamura et al 2013). Residues are color-coded by blosum62 score matrix similarity  
1404 (threshold = 5); residues with 100% similarity are represented in green, 80-100% in gold,  
1405 60-80% in yellow, and less than 60% in white. The Mn-coordinating residues within the  
1406 *Fe-Mn SOD* alignment are indicated (G-77 and Q-146). The percent similarity of *RBCL*  
1407 amino acid residues between contigs and reference sequences are presented in  
1408 Supplemental Table 3.

Figure 01.TIF

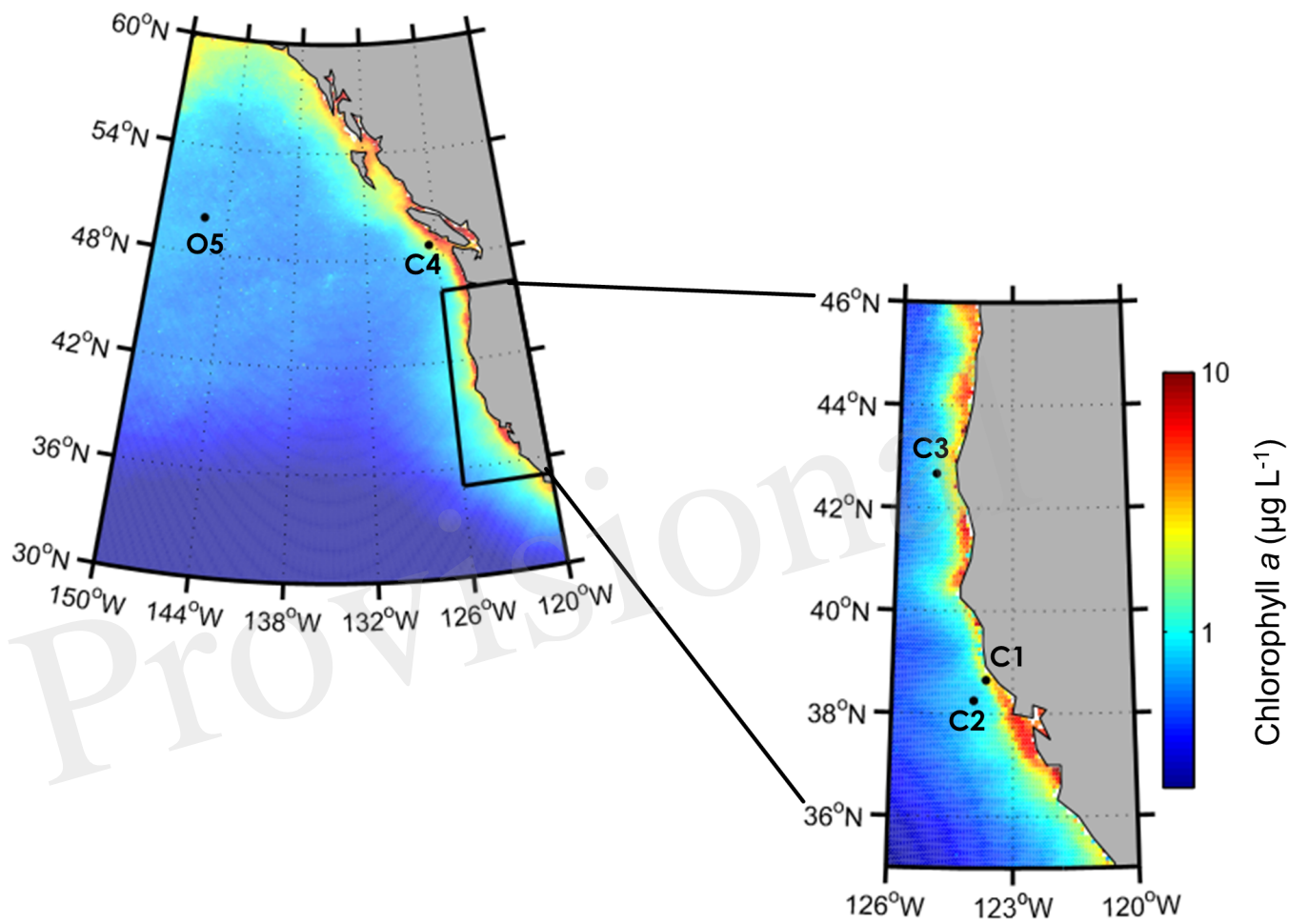


Figure 02.TIF

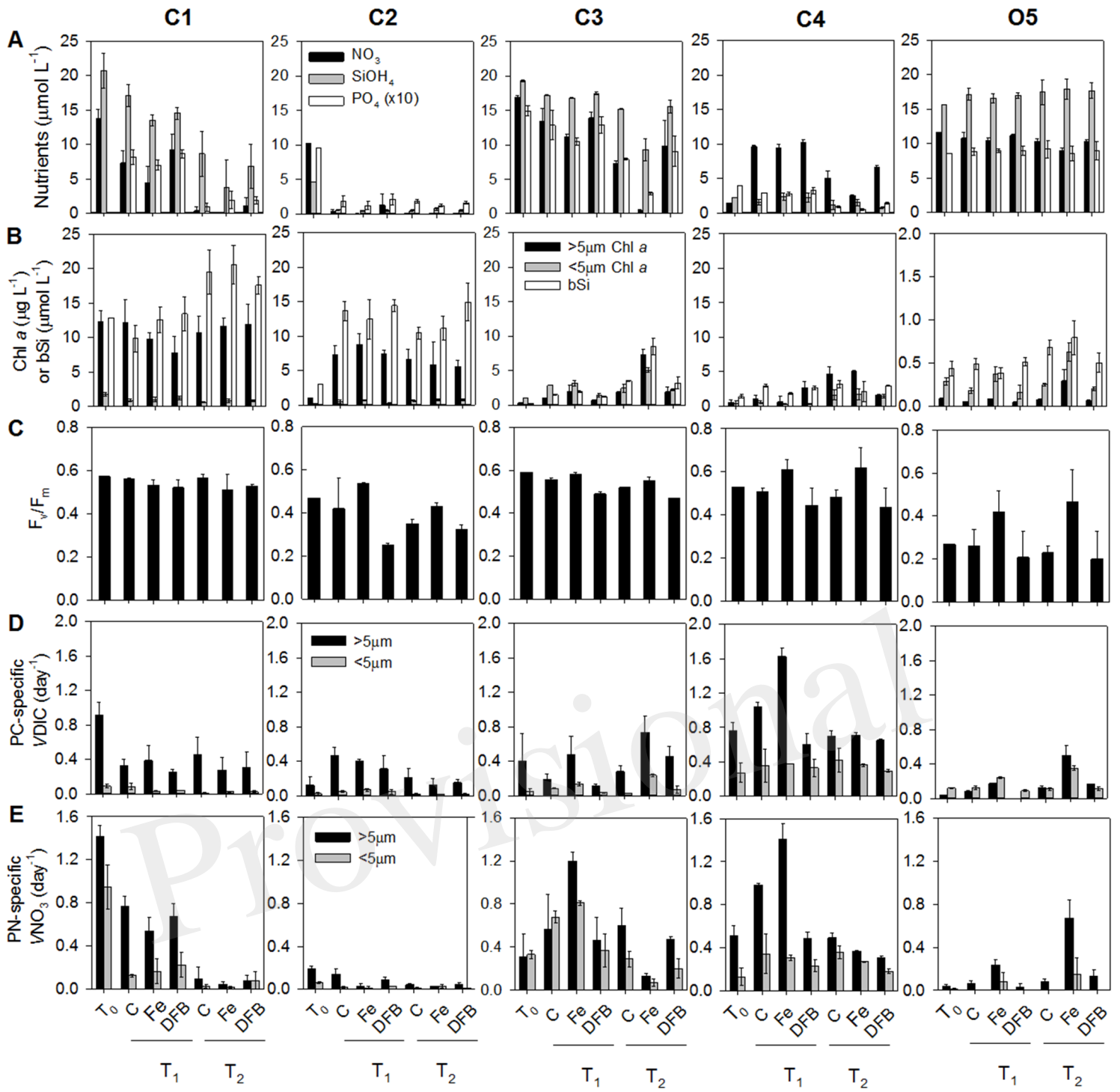


Figure 03.TIF

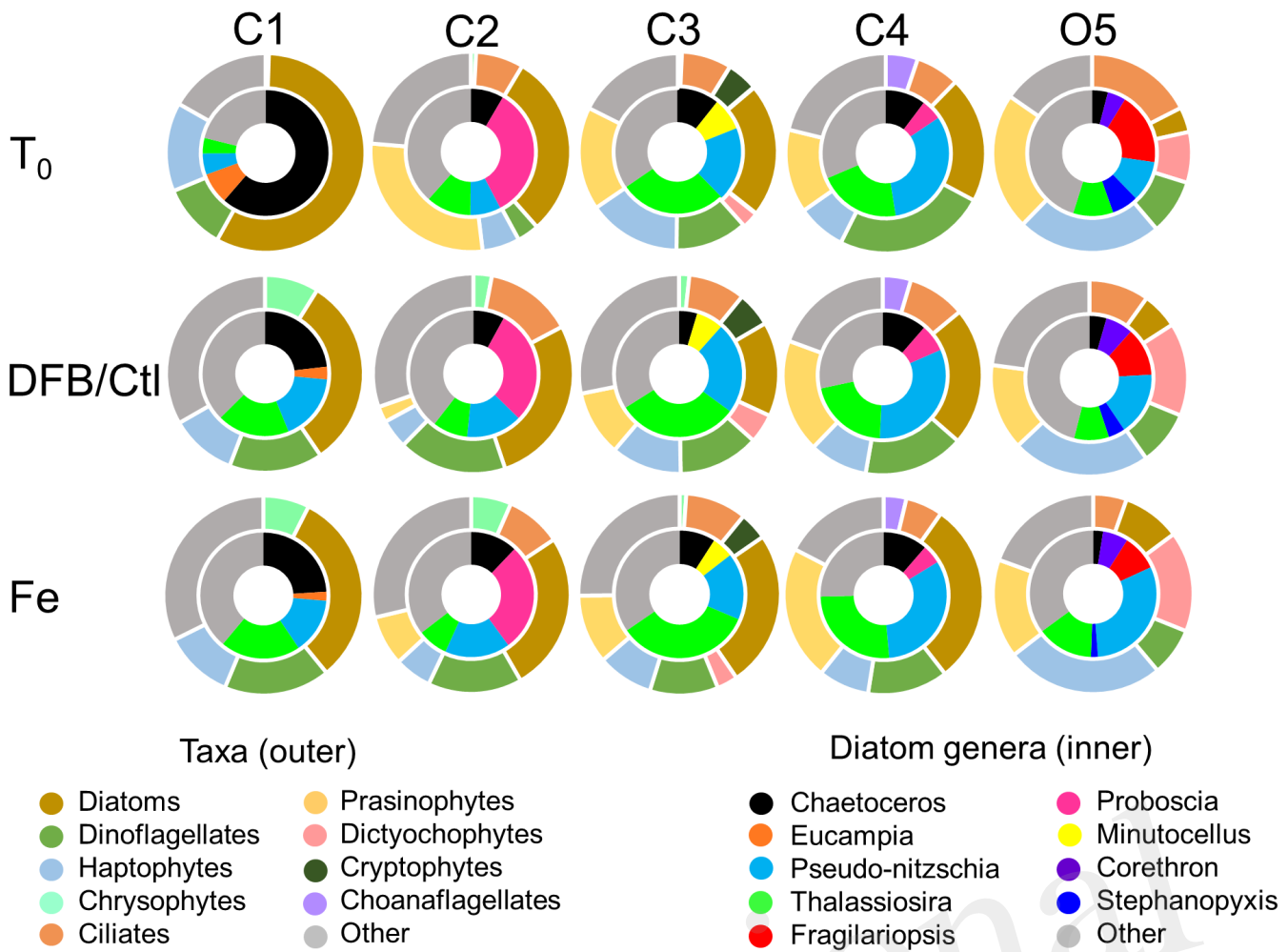


Figure 04.TIF

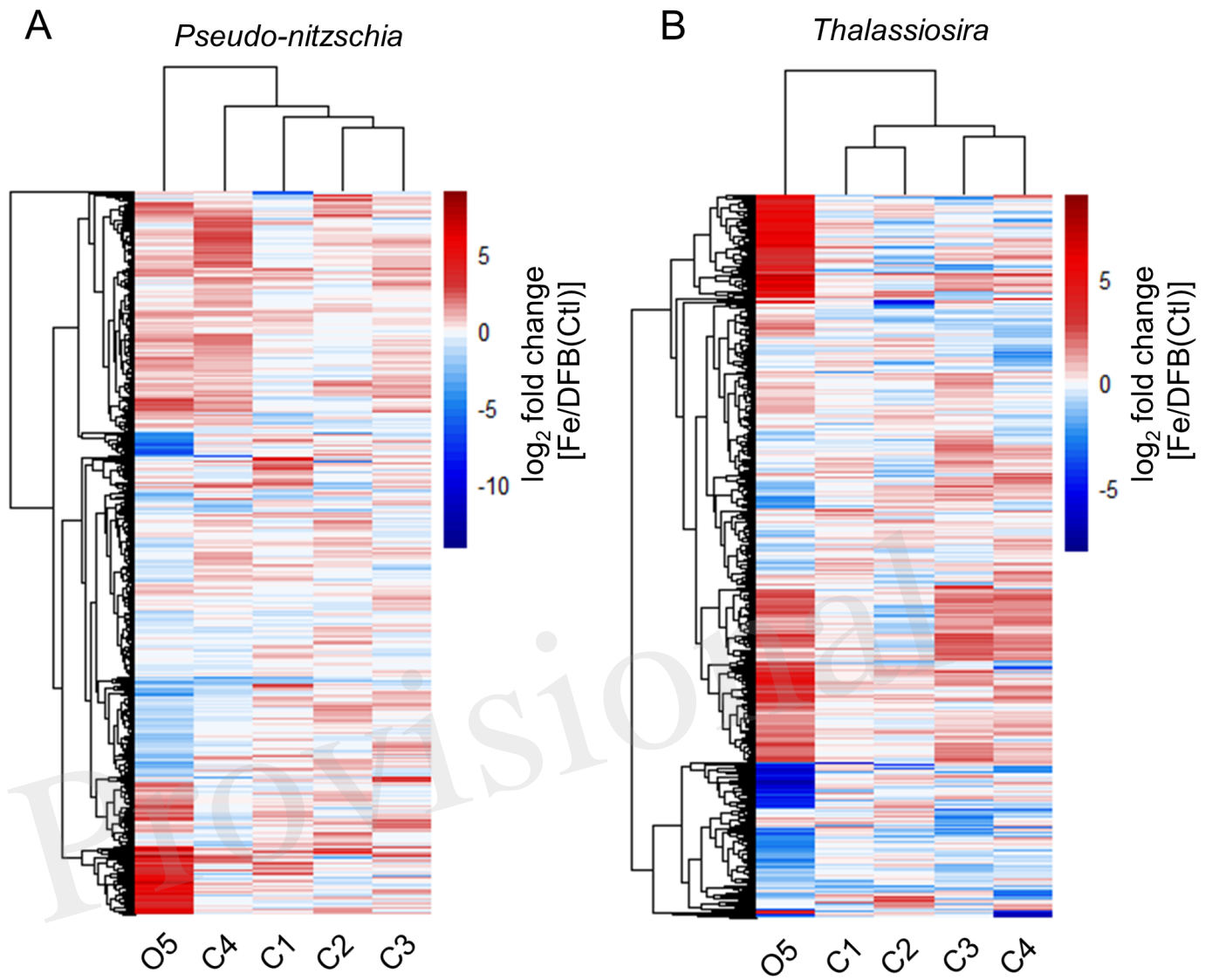


Figure 05.TIF

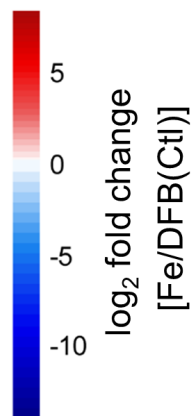
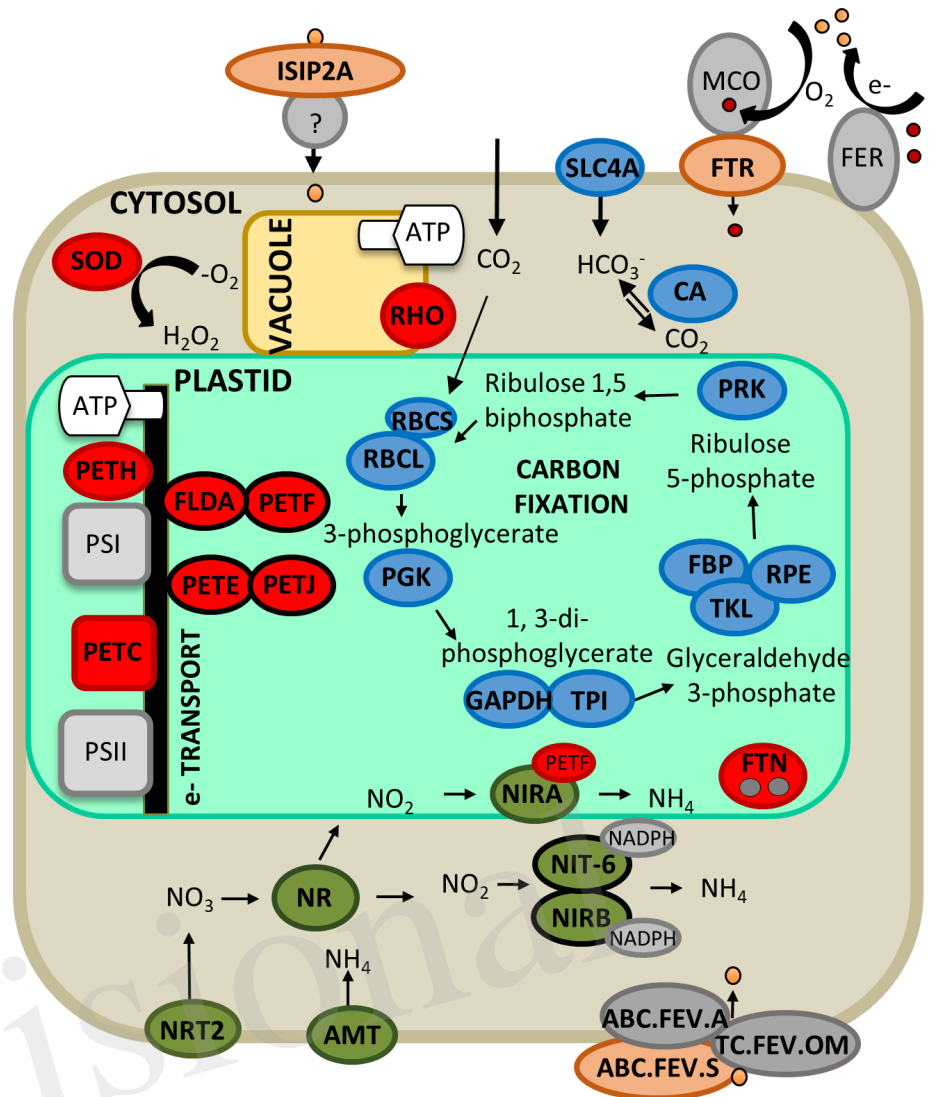
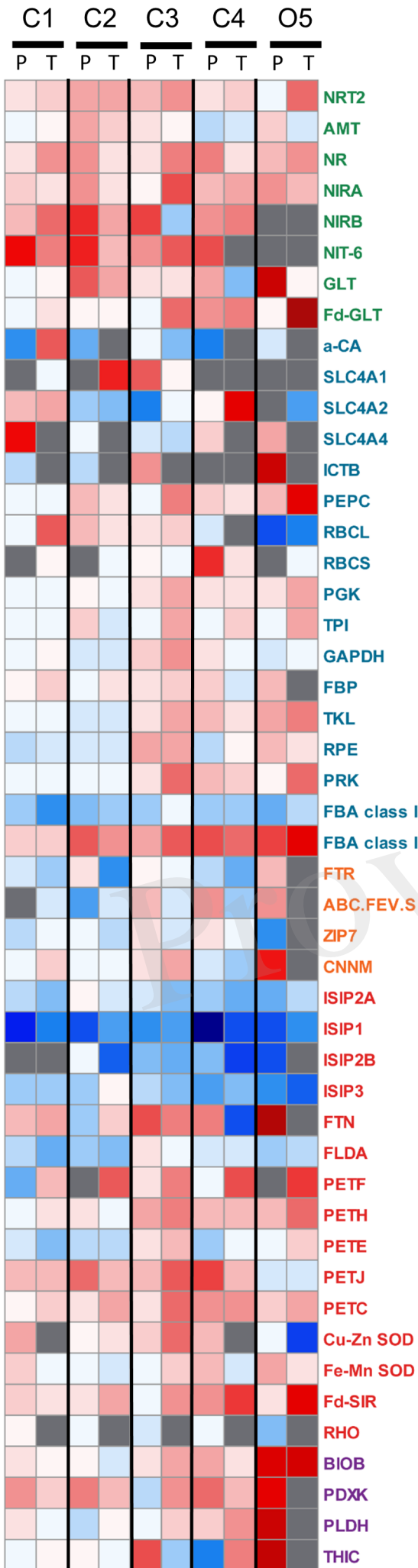


Figure 06.TIF

